ADAPTIVE FINITE ELEMENT BASED SHAPE OPTIMIZATION OF LAMINATED COMPOSITE PLATES WITH CUT-OUTS

by

MOHITE PREETAMKUMAR MARUTRAO

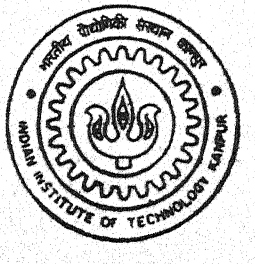

DEPARTMENT OF AEROSPACE ENGINEERING

INDIAN INSTITUTE OF TECHNOLOGY, KANPUR

February, 2001

ADAPTIVE FINITE ELEMENT BASED SHAPE OPTIMIZATION OF LAMINATED COMPOSITE PLATES WITH CUT-OUTS

A thesis Submitted

in Partial fulfilment of the Requirements

for the Degree of

Master of Technology

by

MOHITE PREETAMKUMAR MARUTRAO

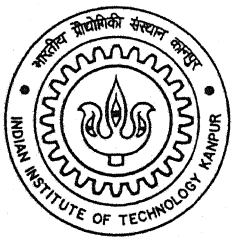

to the

DEPARTMENT OF AEROSPACE ENGINEERING

INDIAN INSTITUTE OF TECHNOLOGY, KANPUR

February 2001

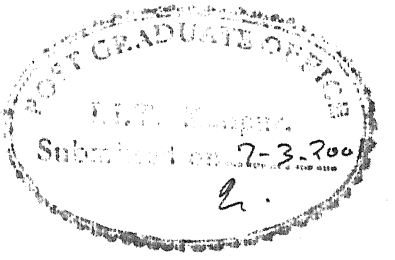

CERTIFICATE

It is certified that work contained in this thesis titled **Adaptive finite element based shape optimization of laminated composite plates with cut-outs**, by **Mohite Preetamkumar Marutrao**, has been carried out under my supervision and that this work has not been submitted elsewhere for a degree.

C. S. Upadhyay

Dr. C. S. Upadhyay
Assistant Professor
Department of Aerospace Engineering
Indian Institute of Technology
Kanpur

February, 2001

ABSTRACT

Optimal design of laminated composite plates with cut-outs is a topic of immense interest to the Aerospace industry, where the goal is to reduce structural weight. Several criteria have to be taken into account before the final "optimal" shape of the cut-out can be reached, i.e. ply failure, buckling, natural frequency, etc. Several studies have been reported in the literature for shape optimization problems. However, the final "optimal" shape will be meaningful only when constraints and objective functions, are evaluated with acceptable accuracy. Thus, a methodology to estimate error in the respective quantity of interest has to be incorporated in the analysis. Further, tools for mesh refinement, in order to control the error in the quantities of interest have to be employed in order to guarantee a reliable design.

This study is a first step towards a reliable shape optimization package, for laminated plate structures. For a fixed higher order plate model, a simple a-posteriori stress recovery algorithm has been developed. The recovered stress is employed to estimate the error in the finite element stress, and to calculate the energy norm of the error in the solution. The effect of higher approximation order, and mesh refinement on the quality of the obtained solution quantities (e.g. stress components and displacements) is studied in detail. It is observed that higher order approximations, along with mesh refinement, is required to obtain pointwise stress information accurately. A detailed comparison of the stresses obtained from the recovery procedure, as compared to three-dimensional results has been carried out for a few sample cases. The recovery is seen to be accurate. The shape of the cut-out is then optimized, with the weight as the objective function and the first-ply failure criterion as the constraint. It is observed that control of the discretization error (via adaptivity) leads to vastly different final designs, as compared to those obtained using reasonably refined meshes, but without adaptivity. It is observed that without adaptivity, the design obtained is unsafe, as more material removal is predicted, as compared to that obtained using adaptivity.

ACKNOWLEDGEMENTS

On this great day, I take opportunity to express my gratitude and heartfelt thanks and appreciations to my supervising professor, Dr. C. S. Upadhyay for his continuous guidance, support and encouragement in carrying out this work. Without him this day was mere a dream for me. His deep involvement, persistence, patience and motivation were pivotal in the sucessful completion of this thesis. I am grateful to him for giving me freedom at work and moral support in my tough days.

His art of explaining doubts for umpteenth number of times, no matter how silly they were, and patience are the qualities to be cherished. His sound computational knowledge and mastery over various subjects relieved me quite often from embarrasing situations during this work. This envigorated my interest in computational solid mechanics, broadened my perspective and helped me become more pragmatic. As a human being, he is benevolent, philanthropic and very friendly, jovial in nature. I shall be proud of myself if I can imbue some of his virtues in my life.

I am thankful to Dr. N. G. R. Iyengar and Dr. C. Venkatesan, whose courses and discussions helped in comprehending the thesis in better manner. I am grateful to Dr. C. Venkatesan for his moral support in my tough days. I am thankful to Dr. V. K. Gupta for forwarding me to Dr. Upadhyay. I am thankful to Singhji, Nazirji for their useful discussions with me.

I am thankful to all of my friends and Sreejith, Andrenathan, Ronnie. The help of Master Masa, Hridyanand Bhaiyyaji during initial stag of thesis is unforgottable. The preparations for exams. with Ramchandra was a nice experience. I am thankful to Lalmoni for his brotherly nature. I will fail in my duties if I forget Bittu Phaniraj. Without playing pranks on him, my each day was meaningless. I am proud to have such a wonderful friends and colleagues who made my stay at IITK an enthralling experience.

I am proud of my parents and other family members for their inspiration and sacrifices to achieve this goal. I am grateful to Kaka, Mavashi and cousines for their loving support.

Mohite P. M.

Contents

List of Figures

List of Tables

LIST OF SYMBOLS

x, y, z	Caretsian coordinates
X, Y, h	Length,width and thickness of the plate
a, b	Semi major and minor axes of elliptical cutout
θ	Orientation of major axis of ellipse with x-axis
NL	Number of layers
h_i	Thickness of i^{th} lamina
α_i	Orientation of i^{th} lamina
$\{\delta\}$	Generalized displacement vector
$[Q_i]$	Material stiffness matrix for i^{th} lamina
$[\bar{Q}_i]$	Transformed material stiffness matrix for i^{th} lamina
N_x, N_y, N_{xy}	Stress resultants
M_x, M_y, M_{xy}	Moment resultants
M_x^*, M_y^*, M_{xy}^*	Moment resultants
Q_x, Q_y	Shear stress resultants
Q_x^*, Q_y^*	Higher order shear stress resultants
$[D_m]$	Membrane rigidity matrix
$[D_b]$	Flexure rigidity matrix
$[D_c]$	Coupling rigidity matrix
$[D_s]$	Shear rigidity matrix
$[D_r]$	Overall rigidity matrix
$\{\epsilon_0\}$	Mid surface strains
k_x, k_y	Mid surface curvatures
k_x^*, k_y^*, ν, ν^*	Higher order terms
U	Potential energy
$[K]$	Stiffness matrix
W	Weight of the laminate
T_x, T_y, T_{xy}	Applied inplane loads

Chapter 1

INTRODUCTION

1.1 GENERAL

> **"Reliability of the constraints in shape optimization effects the final optimal shape."**
>
> Constraint evaluation plays the main role in any optimization problem. If the evaluated constraints itself are inaccurate then the final optimal solution, obviously, represents a false picture, which is dangerous in the design process. Hence, before proceeding for any optimization procedure one should have enough confidence in the evaluated constraint. Overestimation is always better than underestimation.

Composite materials are now well established and widely used in structural applications within the aerospace, automobile and other high performance industries where weight reduction and directional properties are the main criteria. Cut-outs are unavoidable in structures like aircrafts. They are used for door openings and windows in the fuselage, flow passages, wiring connections, bolting, assembly purpose etc. Sometimes cut-outs are used merely to reduce the structural weight like in the web members of aircraft wings. Aircraft structures are subjected to complex situation of loadings, like Aerodynamic loads, Maneuvering loads, friction loads, etc. In general,

these structures are weight sensitive and reliability stringent. The design of light weight and safe laminated composite plates with cut-outs has thus become an important topic of research. Here, an attempt is made to optimize the cut-out shape in moderately thick composite laminated plates for minimum weight design with first-ply failure criterion as a constraint. The effect of mesh refinement on the quality of the computed stresses, and hence the failure criterion will also be discussed.

1.2 REVIEW OF THE STATE OF THE ART

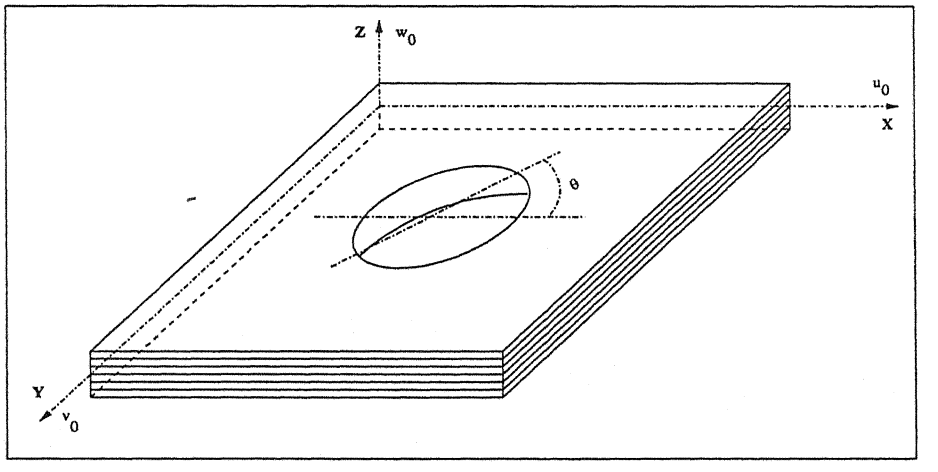

Figure 1.1: Laminated plate with cut-out

Here, an attempt is made to demonstrate the effect of reliability of constraints on the final optimal solution. Initially, we start with a given circular hole and optimize its final shape for minimum weight subjected to constraints, i.e. Tsai-Wu failure criterion, without considering reliability of the computed data.The process is then repeated with a control on the reliability of the computed data, i.e. effect of adaptivity on final optimal shape.

Many researchers have attempted to optimize the composite laminate for design variables like ply thickness and ply orientation in order to obtain minimum

weight designs subjected to several constraints, such as maximum strength, maximum stress, first ply failure load (or reliability requirements) etc. (see [1]- [8]). The optimum design of laminated plates for maximum buckling load has also been attempted (see [9]- [11]) with constraints on the natural frequency. Others have worked on the optimization of composite plates with a cut-out (see [12], [13]). Limited literature is available on shape optimization of composite structures (see [14], [15]). Botkin [14] has worked on shape optimization of the stamped sheet metal parts with buckling and stress constraints. Sivakumar et al [15] have worked on optimization with dynamic constraints. Generally, the focus in all the studies mentioned above has been to demonstrate the effect of optimization on the final design. Thus, a fixed finite element mesh has been used, with quadratic approximation, to obtain the results. The effect of the discretisation error on the final optimal design has not been discussed.

1.3 LAYOUT OF THESIS

The organisation of the thesis is given as:

1. The first chapter deals with a discussion on the state-of-the-art and the goals of this study.
2. The second chapter is devoted to a discussion of the plate model and energy formulation.
3. The third chapter deals with the finite element formulation of the problem.
4. The fourth chapter explains the recovery based a-posteriori error estimator for laminated plates. It is then followed by adaptive technique employed for reliable constraints evaluation.
5. The fifth chapter deals with optimization problem formulation, optimization technique and explains the Tsai-Wu failure criterion.
6. In the sixth chapter, first we present validation results for the plate model and Tsai-Wu failure criterion followed by other numerical results and inferences from our study.

7. Finally, in the seventh chapter, we have presented the conclusions made from our study and discussion on the future scope of this work.

Chapter 2

HIGHER ORDER PLATE THEORY

The analysis of laminated plates is based on the choice of a plate theory. Several plate theories have been developed (see [7], [8], [15]), with assumed variation of the displacement field in the transverse direction. Below we present the details of one such plate theory due to Kant et al [16].

2.1 DEFINITION OF DISPLACEMENT FIELDS

Symmetric laminates find many applications in the aircraft industry. Although symmetric laminates are simple to analyse and design, some specific applications of laminated composites require unsymmetric laminates. For example, the coupling between bending and extension exhibited by this type of laminates is an essential feature of jet turbine fan blades with pretwist. It can be noted that the theories for unsymmetric laminates are applicable to symmetric laminates as a special case. Unlike symmetric laminates, unsymmetric laminates exhibits the membrane-flexure coupling phenomenon, which necessitates the use of a displacement field containing

both, membrane as well as flexure deformation terms which contribute to the overall response of a laminate. Thus, to begin with, the displacement field

$$\{V(x,y,z)\} = [\, u(x,y,z),\ v(x,y,z),\ w(x,y,z)\,]^T$$

is derived from the expanded Taylor's series in terms of thickness coordinate z. This is given as (see [16] for details):

$$\begin{aligned} u(x,y,z) &= u_0(x,y) + z\theta_x(x,y) + z^2\phi_x(x,y) + z^3\psi_x(x,y); \\ v(x,y,z) &= v_0(x,y) + z\theta_y(x,y) + z^2\phi_y(x,y) + z^3\psi_y(x,y); \\ w(x,y,z) &= w_0(x,y) \end{aligned} \tag{2.1}$$

In the expansion (2.1), it is assumed that transverse normal strain ϵ_{zz} is zero.
The linear strain-displacement relationships using small deformation theory can be written as follows:

$$\begin{aligned} \epsilon_{xx} &= u_{0,x} + z\,\theta_{x,x} + z^2\,\phi_{x,x} + z^3\,\psi_{x,x}; \\ \epsilon_{yy} &= v_{0,y} + z\,\theta_{y,y} + z^2\,\phi_{y,y} + z^3\,\psi_{y,y}; \\ \gamma_{xy} &= u_{0,y} + z\,\theta_{x,y} + z^2\,\phi_{x,y} + z^3\,\psi_{x,y} \\ &\quad + v_{0,x} + z\,\theta_{y,x} + z^2\,\phi_{y,x} + z^3\,\psi_{y,x}; \\ \gamma_{yz} &= \theta_y + 2\,z\,\phi_y + 3\,z^2\,\psi_y + w_{0,y}; \\ \gamma_{xz} &= \theta_x + 2\,z\,\phi_x + 3\,z^2\,\psi_x + w_{0,x} \end{aligned} \tag{2.2}$$

where comma (,) denotes the partial derivatives.

The condition that the transverse shear stresses vanish on the plate's top and bottom faces (see Fig. 2.1) is equivalent to the requirement that the corresponding strains be zero on these surfaces, i.e.

$$\gamma_{yz}(x,y,\pm\tfrac{h}{2}) = \gamma_{xz}(x,y,\pm\tfrac{h}{2}) = 0$$

On introduction of the conditions as given above in the expressions for transverse shear strains, the following relations are obtained.

$$\begin{aligned} &\phi_x = \phi_y = 0 \quad \text{and} \\ &\psi_y = -\tfrac{4}{3h^2}(\theta_y + w_{0,y})\ ; \quad \psi_x = -\tfrac{4}{3h^2}(\theta_x + w_{0,x}) \end{aligned} \tag{2.3}$$

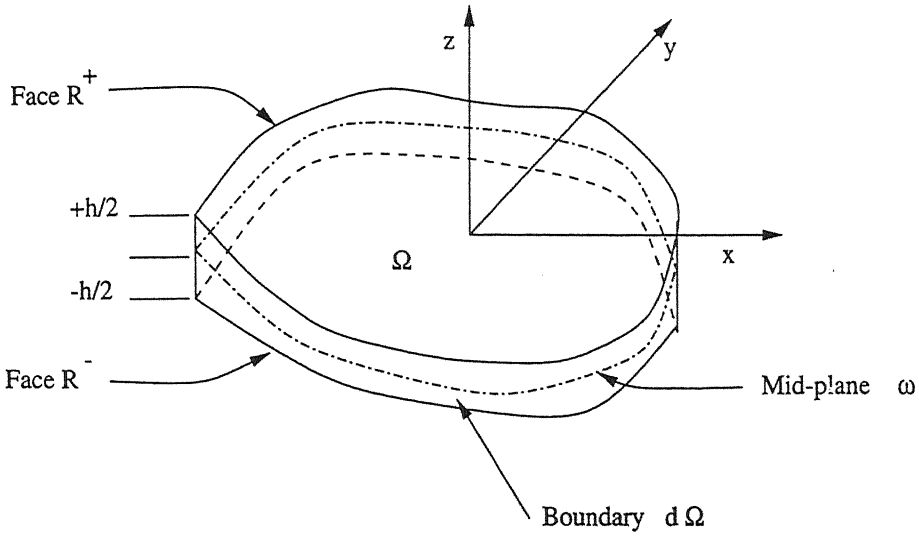

Figure 2.1: Representation of arbitrary three dimensional domain

The displacement field of Eq. (2.1) is modified by setting ϕ_x and ϕ_y to be zero according to conditions of Eq. (2.3). The resulting displacement field is written below:

$$\begin{aligned} u(x,y,z) &= u_0(x,y) + z\,\theta_x(x,y) + z^3\,\psi_x(x,y); \\ v(x,y,z) &= v_0(x,y) + z\,\theta_y(x,y) + z^3\,\psi_y(x,y); \\ w(x,y,z) &= w_0(x,y) \end{aligned} \tag{2.4}$$

In Eq. (2.4) u, v and w are the displacements along x, y and z directions respectively. u_0, v_0 and w_0 are the mid-plane displacements while θ_x, θ_y are rotations about y and x axes, respectively. Whereas, ψ_x and ψ_y are higher order terms in the Taylor's series expansion and are also defined at mid-plane. Thus, the generalised displacement vector $\{\delta\}$ of the mid-surface contains seven degrees of freedom (DOF) and is given by:

$$\{\delta\} = \{u_0, v_0, w_0, \theta_x, \theta_y, \psi_x, \psi_y\}^T.$$

The corresponding strain-displacement relationship are:

$$\begin{aligned}
\epsilon_{xx} &= u_{0,x} + z\,\theta_{x,x} + z^3\,\psi_{x,x};\\
\epsilon_{yy} &= v_{0,y} + z\,\theta_{y,y} + z^3\,\psi_{y,y};\\
\gamma_{xy} &= u_{0,y} + z\,\theta_{x,y} + z^3\,\psi_{x,y}\\
&\quad + v_{0,x} + z\,\theta_{y,x} + z^3\,\psi_{y,x};\\
\gamma_{yz} &= \theta_y + 3\,z^2\,\psi_y + w_{0,y};\\
\gamma_{xz} &= \theta_x + 3\,z^2\,\psi_x + w_{0,x}
\end{aligned} \tag{2.5}$$

2.2 LAMINATE CONSTITUTIVE EQUATIONS

A unidirectional fibre reinforced lamina is treated as an orthotropic material whose material symmetry planes are parallel and transverse to the fiber direction.

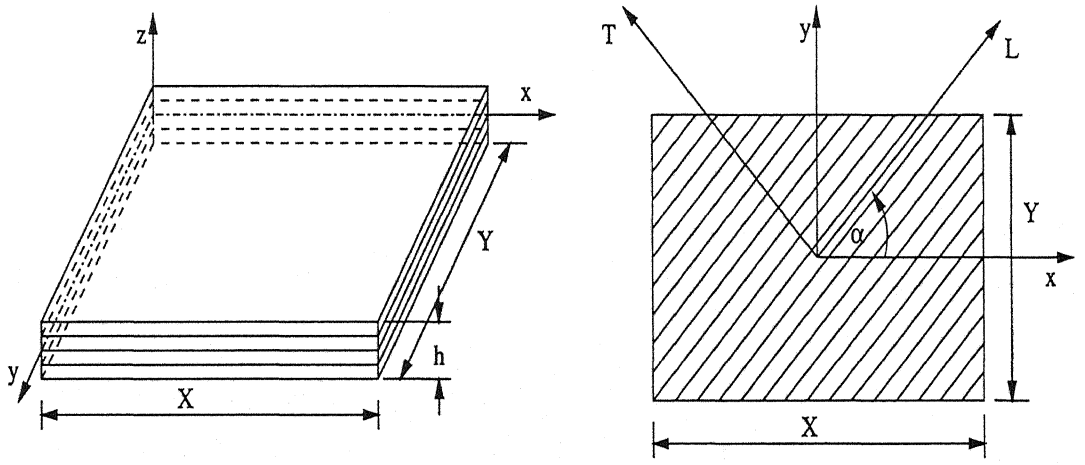

Figure 2.2: Co-ordinate axes in lamina

Following fig. (2.2) the material co-ordinates axes L and T are defined parallel and perpendicular to the fibre direction respectively, while global co-ordinates are x and y. The angle between global co-ordinate axis x and fibre direction, material co-ordinate axis L, is α and is known as the orientation angle. As a sign convention anticlockwise angle is taken as positive.

Generalized Hooke's law

In the formulation of lamina constitutive equation the following two assumptions are made.

1. The lamina is a continuum.
2. It behaves as a linearly elastic material.

Further, at the micro-level the following assumptions are made about the material:

1. Perfect bonding between fibres and matrix exists.
2. Fibres are parallel and uniformly distributed throughout.
3. The matrix is free of voids or micro cracks and initially in a stress free state.
4. Both fibres and matrix are isotropic and obey Hook's law.

Stress-strain relations for the l^{th} lamina in the material coordinate axis, whose fibers are oriented at an angle α with reference to the x axis is given as ([17], [18]):

$$\left\{ \sigma_i \right\}_l = [\bar{Q}_{ij}]_l \left\{ \epsilon_j \right\}_l \tag{2.6}$$

where $\{\sigma_i\}$ is the vector of stress components, $[\bar{Q}_{ij}]$ is the stiffness matrix, and $\{\epsilon_j\}$ are the engineering strain components, for the l^{th} lamina.
The stresses and strains in the x, y and z directions are obtained by transformation of the relations given in equation (2.6). The transformed stress strain relations for the l^{th} lamina are given as:

$$\begin{Bmatrix} \sigma_x \\ \sigma_y \\ \tau_{xy} \\ \tau_{yz} \\ \tau_{xz} \end{Bmatrix}_l = \begin{bmatrix} \bar{Q}_{11} & \bar{Q}_{12} & \bar{Q}_{16} & 0 & 0 \\ \bar{Q}_{21} & \bar{Q}_{22} & \bar{Q}_{26} & 0 & 0 \\ \bar{Q}_{16} & \bar{Q}_{26} & \bar{Q}_{66} & 0 & 0 \\ 0 & 0 & 0 & \bar{Q}_{44} & \bar{Q}_{45} \\ 0 & 0 & 0 & \bar{Q}_{45} & \bar{Q}_{55} \end{bmatrix}_l \begin{Bmatrix} \epsilon_x \\ \epsilon_y \\ \gamma_{xy} \\ \gamma_{yz} \\ \gamma_{xz} \end{Bmatrix}_l \tag{2.7}$$

Using the above lamina constitutive equations and integrating the stresses over the laminate thickness, the stress resultants in terms of inplane forces, moments and

shear forces per unit length, for a laminate with NL laminae are,

$$\begin{Bmatrix} \{\mathrm{N}\} \\ \{\mathrm{M}\} \\ \{\mathrm{M}^*\} \\ \{\mathrm{Q}\} \\ \{\mathrm{Q}^*\} \end{Bmatrix} = \begin{bmatrix} [D_m] & [D_c] & [0] \\ [D_c]^T & [D_b] & [0] \\ [0] & [0] & [D_s] \end{bmatrix} \begin{Bmatrix} \{\epsilon_0\} \\ \{\kappa\} \\ \{\kappa^*\} \\ \{\nu\} \\ \{\nu^*\} \end{Bmatrix} \tag{2.8}$$

(Detailed expansion of Eq. (2.8) is given in Appendix A.)

where $\{\epsilon_0\}$ are the mid-plane strains, $\{\kappa\}$ are the mid-surface curvatures and $\{\kappa^*\}$, $\{\nu\}$, $\{\nu^*\}$ are higher order terms and

$$\{\mathrm{N}\}^{\mathrm{T}} = (N_x, N_y, N_{xy}) = \sum_{l=1}^{NL} \int_{z_l}^{z_{l-1}} (\sigma_x, \sigma_y, \sigma_{xy})^l \quad dz; \tag{2.9}$$

$$\{\mathrm{M}\}^{\mathrm{T}} = (M_x, M_y, M_{xy}) = \sum_{l=1}^{NL} \int_{z_l}^{z_{l-1}} (\sigma_x, \sigma_y, \sigma_{xy})^l \; z \; dz; \tag{2.10}$$

$$\{\mathrm{M}^*\}^{\mathrm{T}} = (M_x^*, M_y^*, M_{xy}^*) = \sum_{l=1}^{NL} \int_{z_l}^{z_{l-1}} (\sigma_x, \sigma_y, \sigma_{xy})^l \; z^3 \; dz; \tag{2.11}$$

$$\{\mathrm{Q}\}^{\mathrm{T}} = (Q_x, Q_y) = \sum_{l=1}^{NL} \int_{z_l}^{z_{l-1}} (\tau_{xz}, \tau_{yz})^l \quad dz; \tag{2.12}$$

$$\{\mathrm{Q}^*\}^{\mathrm{T}} = (Q_x^*, Q_y^*) = \sum_{l=1}^{NL} \int_{z_l}^{z_{l-1}} (\tau_{xz}, \tau_{yz})^l \; z^2 \; dz. \tag{2.13}$$

Here, z_i are the z coordinates corresponding to the laminae interfaces as shown in fig 2.3.

The other terms and corresponding rigidity matrices are given in Appendix A.

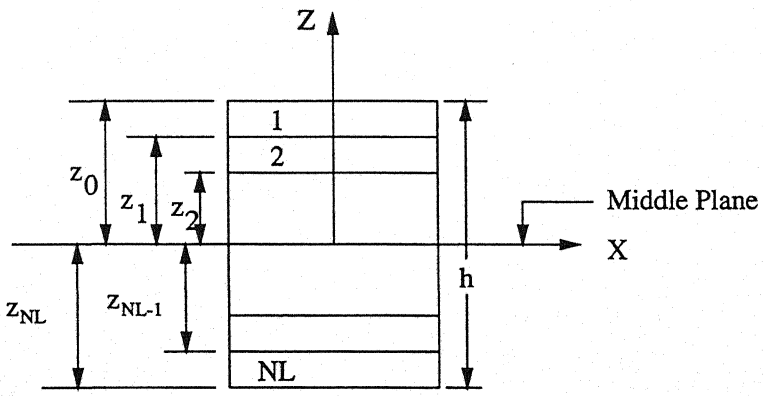

Figure 2.3: Geometry of multilayered laminate

Thus, with the assumed displacement model, the various rigidity matrices derived are:

$[D_m]$ = Membrane; $[D_c]$ = Membrane-flexure coupling.

$[D_b]$ = Flexure; $[D_s]$ = Shear.

The set of rigidity matrices $[D_m], [D_c], [D_b]$ and $[D_s]$ are used in forming overall rigidity matrix $[D_r]$ for the laminate.

Chapter 3

FINITE ELEMENT FORMULATION

Triangular elements are used in the finite element approximation employed in this study, along with hierarchic shape functions of order p ($p \leq 4$). The mesh generation is done using advancing front method based automatic mesh generator. A mesh generated over the plate domain is shown in fig. 3.1. Below, we give the finite element formulation for the chosen plate model.

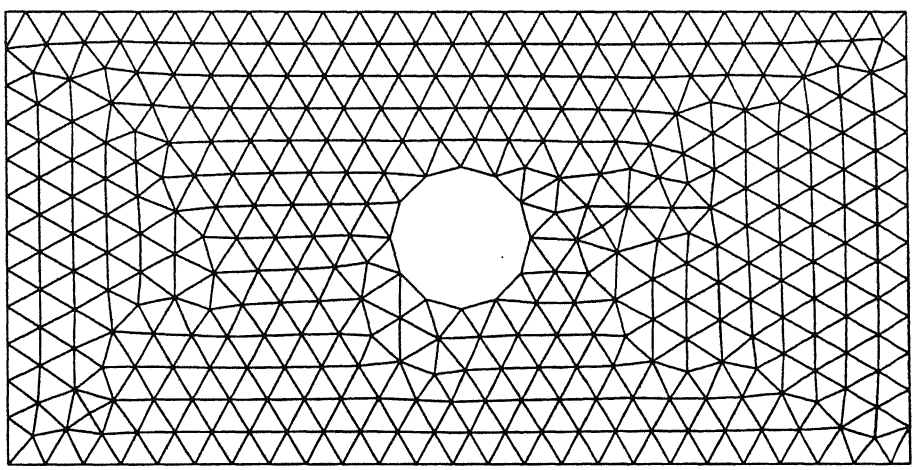

Figure 3.1: Rectangular domain with circular cut-out, meshed with an advancing front method based mesh generator.

3.1 DEFINITIONS

Let $\{V\}$ be the displacement vector defined as:

$$\{V\} = \begin{Bmatrix} u \\ v \\ w \end{Bmatrix} \tag{3.1}$$

Let the stress and strain vectors corresponding to $\{V\}$ be $\{\sigma\}$ and $\{\epsilon\}$ which can be defined as:

$$\{\sigma\} = \begin{Bmatrix} \sigma_x \\ \sigma_y \\ \tau_{xy} \\ \tau_{yz} \\ \tau_{xz} \end{Bmatrix} \qquad \{\epsilon\} = \begin{Bmatrix} \epsilon_x \\ \epsilon_y \\ \gamma_{xy} \\ \gamma_{yz} \\ \gamma_{xz} \end{Bmatrix} \tag{3.2}$$

From the generalized Hooke's law which relates stress components to the respective strain components in global coordinate system

$$[\sigma] = [\bar{Q}]\,\{\epsilon\} \tag{3.3}$$

where material stiffness matrix $[\bar{Q}]$ for orthotropic material is as given in Eq. (2.7) for each lamina.

For any elastic body, the linear strain-displacement relationships using small deformation theory is given in Eq. (2.5).

The above relations can be expressed in matrix form as:

$$\{\epsilon\} = [\bar{D}]\,\{V\} \tag{3.4}$$

where $[\bar{D}]$ is a differential operator in terms of global coordinates such that

$$[\bar{D}] = \begin{bmatrix} \frac{\partial}{\partial x} & 0 & 0 \\ 0 & \frac{\partial}{\partial y} & 0 \\ \frac{\partial}{\partial y} & \frac{\partial}{\partial x} & 0 \\ 0 & \frac{\partial}{\partial z} & \frac{\partial}{\partial y} \\ \frac{\partial}{\partial z} & 0 & \frac{\partial}{\partial x} \end{bmatrix} \tag{3.5}$$

The components of displacement can be written in terms of the seven unknown in-plane functions, which can be written as:

$$\{\delta\}^T = \{u_0, v_0, w_0, \theta_x, \theta_y, \psi_x, \psi_y\}$$

The displacement vector is written in matrix form as

$$\{V\} = [\Phi]\ \{\delta\} \tag{3.6}$$

where

$$[\Phi] = \begin{bmatrix} 1 & 0 & 0 & z & 0 & z^3 & 0 \\ 0 & 1 & 0 & 0 & z & 0 & z^3 \\ 0 & 0 & 1 & 0 & 0 & 0 & 0 \end{bmatrix} \tag{3.7}$$

In the finite element approximation the functions u_0, v_0, ... etc are approximated using n shape functions per element.

$$\begin{Bmatrix} u_0 \\ v_0 \\ w_0 \\ \theta_x \\ \theta_y \\ \psi_x \\ \psi_y \end{Bmatrix} = \sum_{i=1}^{n} N_i \begin{Bmatrix} u_{0i} \\ v_{0i} \\ w_{0i} \\ \theta_{xi} \\ \theta_{yi} \\ \psi_{xi} \\ \psi_{yi} \end{Bmatrix} \tag{3.8}$$

$$\{\delta\} = \sum_{i=1}^{n} N_i\ \{\delta_i\} \tag{3.9}$$

where, $n = (p+1)\ (p+2)/2$ is the number of independent coefficients in an element, p is the approximation order, N_i is the i^{th} shape function associated with i^{th} independent coefficient in terms of normalised coordinates ξ and η and $\{\delta_i\}$ is the generalized displacement vector corresponding to i^{th} independent coefficient of an element.

Remark: When Lagrangian shape functions are used, the independent coefficients correspond to physical nodes.

Hence displacement vector can be written as

$$\{V\} = [\Phi]\ [N]\ \{d\} \tag{3.10}$$

where $\{d\}^T = \{\{\delta_1\}^T, \{\delta_2\}^T, ...\{\delta_n\}^T\}$ and $[N]$ is a matrix in terms of n inplane hierarchic shape functions given in *Appendix B*.

Hence, the strain vector can be written as

$$\{\epsilon\} = ([\bar{D}]\ [\Phi]\ [N])\ \{d\} \tag{3.11}$$

and the stress vector

$$\{\sigma\} = [\bar{Q}]\ ([\bar{D}]\ [\Phi]\ [N])\ \{d\} \tag{3.12}$$

3.2 FINITE ELEMENT FORMULATION USING ENERGY PRINCIPLE

The total potential for the plate is given by

$$\Pi\ (\delta) = \sum_{e=1}^{N} \pi^e\ (\delta), \tag{3.13}$$

where π^e is the total potential of the non-intersecting (but adjacent) sub-domains e which are part of the domain (N sub-domains are considered here). The total potential can be expressed in terms of internal strain energy $U^{(e)}$ and external work done $W^{(e)}$, as follows:

$$\pi^e\ (\delta) = U^{(e)} - W^{(e)}. \tag{3.14}$$

Strain energy of the laminate can expressed as follows:

$$U^{(e)} = \frac{1}{2} \int_{V^{(e)}} \{\epsilon\}^T\ [\sigma]\ dV^{(e)} \tag{3.15}$$

Work done by the applied external transverse load is,

$$\begin{aligned} W^{(e)} &= \int_{A^{(e)}} \{V\}^T_{z=\pm\frac{h}{2}}\ f\ dA^{(e)} \\ &= \int_{R^{+(e)}} w_0\ f^+\ dA^{(e)} + \int_{R^{-(e)}} w_0\ f^-\ dA^{(e)} \end{aligned} \tag{3.16}$$

where f^+ is the transverse load on the top face R^+ and f^- is the transverse load on the top face R^-.

The exact solution $\{V_{ex}\}$ to this problem is the minimizer of the total potential Π. This can be obtained as:

$$\delta^{(1)}\,\Pi = 0,$$

which is also the *Virtual Work Formulation* of the problem in terms of the components of δ. From this, the seven coupled equilibrium equations in terms of the components of δ can be obtained. This leads to the generalised finite element formulation:

$$[K]\,\{d\} = \{F\} \tag{3.17}$$

where $[K]$ is the global stiffness matrix and $\{F\}$ is global load vector.
In the next section, we are going to employ the virtual work formulation to derive the finite element formulation of this problem.

3.3 COMPUTATION OF ELEMENT STIFFNESS MATRIX

The stiffness matrix corresponding to assumed deformation state of an element can be defined by expressing the internal strain energy in terms of unknown nodal displacements. In the formulation of unsymmetric laminates the membrane, the flexure,membrane-flexure coupling and shear strains contribute to strain energy. The set of Eq. (2.5) can be used along with Eq. (3.12), (3.15) to express these strains in terms of nodal displacements.

The internal strain energy of an element (given by area A^e) can be determined as:

$$\begin{aligned} U^e = \tfrac{1}{2}\int_{A(e)} \big(\{d\}^T \left([B_m]^T [D_m] [B_m] \right) \{d\} + \{d\}^T \left([B_b]^T [D_b] [B_b] \right) \{d\} \\ + \{d\}^T \left([B_s]^T [D_s] [B_s] \right) \{d\} + \{d\}^T \left([B_m]^T [D_c] [B_b] \right) \{d\} \\ + \{d\}^T \left([B_b]^T [D_c] [B_m] \right) \{d\} \big)\, dA \end{aligned} \tag{3.18}$$

Here the first term on the right-hand side of Eq. (3.18) is the in-plane contribution, the second and third terms are out-of-plane bending and through-thickness shearing contributions, respectively. The last two terms are contributions from coupling between in-plane and out-of-plane actions.

The strain energy expression can be written in a concise form as:

$$U^{(e)} = \frac{1}{2} \{d^e\}^T [K^e] \{d^e\} \tag{3.19}$$

where $[K^e]$ is the stiffness matrix and $\{d^e\}$ are the coefficients corresponding to the finite element solution in an element e. All the terms in equation (3.18) are evaluated individually and then summed to yield $[K^e]$.

It is given by:

$$\begin{aligned}[K^e] = \int_{A^e} [\, ([B_m]^T [D_m] [B_m]) + ([B_b]^T [D_b] [B_b]) + ([B_s]^T [D_s] [B_s]) \\ + ([B_m]^T [D_c] [B_b]) + ([B_b]^T [D_c] [B_m]) \,]\, dA\end{aligned} \tag{3.20}$$

Numerical integration is carried out to get the element stiffness matrix.
The matrices $[B_m], [B_b]$ and $[B_c]$ and vector $\{d\}$ are given in *Appendix B*.

3.4 COMPUTATION OF ELEMENT LOAD VECTOR

For the extension and/or bending problems of laminated plates, the applied external forces have been considered to be of the following types:

1. Uniformly distributed load acting over the element in the z-direction on top or bottom bounding planes of the plate.
2. Sinusoidal distributed load acting over the element in the z-direction on top or bottom bounding planes of the plate.
3. Traction load acting along the edges in the x or y-direction .

The total external work done by these forces on an element can be expressed as

follows:

$$W^e = \{d\}^T \int_S ([\Phi]\,[N])^T \{T_r\}\, dS \tag{3.21}$$

or

$$W^e = \{d\}^T \{F^e\} \tag{3.22}$$

where $\{F^e\}$ is the element load vector, and the traction vector is given as:

$$\{T_r\} = \begin{Bmatrix} T_x \\ T_y \\ T_z \end{Bmatrix} \tag{3.23}$$

When the loading is in-plane,

$$\{T_r\} = \begin{Bmatrix} T_x \\ T_y \\ 0 \end{Bmatrix}$$

When the loading is in the transverse direction,

$$\{T_r\} = \begin{Bmatrix} 0 \\ 0 \\ T_z \end{Bmatrix}$$

Transverse loading, T_z, can be sinusoidal as $T_z = P_c \sin(\frac{m\pi x}{X}) \sin(\frac{m\pi y}{Y})$ or uniform pressure $T_z = P_0$. T_x, T_y can be uniform inplane tractions along x and y, respectively.

3.5 GEOMETRIC APPROXIMATION

3.5.1 STRAIGHT EDGE ELEMENTS

The geometry is expressed in terms of the shape functions as:

$$\begin{Bmatrix} x \\ y \end{Bmatrix} = \sum_{i=1}^{3} N_i \begin{Bmatrix} x_i \\ y_i \end{Bmatrix} \tag{3.24}$$

where, $\left\{ \begin{matrix} x_i \\ y_i \end{matrix} \right\}$ are the coordinates of the i^{th} node of the element, and N_i are the linear shape functions of the element.

LINEAR MAPPING:

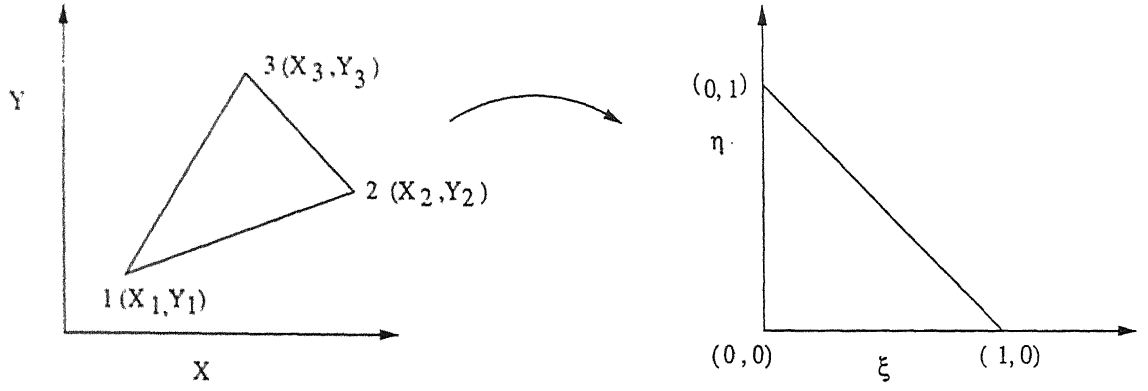

Figure 3.2: Linear mapping in two dimension

Linear mapping in general is used when all sides of mapped elements are straight lines (see fig. 3.2). Consider the mapping of variables from x,y to ξ, η such that $\{x, y \in A\}$ on substitution of N_i these can be written in the matrix form as

$$\left\{ \begin{matrix} x - x_1 \\ y - y_1 \end{matrix} \right\} = \left[\begin{matrix} x_2 - x_1 & x_3 - x_1 \\ y_2 - y_1 & y_3 - y_1 \end{matrix} \right] \left\{ \begin{matrix} \xi \\ \eta \end{matrix} \right\} \tag{3.25}$$

Clearly,

$$\begin{aligned} \frac{\partial x}{\partial \xi} &= x_2 - x_1 & \frac{\partial x}{\partial \eta} &= x_3 - x_1 \\ \frac{\partial y}{\partial \xi} &= y_2 - y_1 & \frac{\partial y}{\partial \eta} &= y_3 - y_1 \end{aligned} \tag{3.26}$$

On inverting the matrix it is easy to see that

$$\left\{ \begin{matrix} \xi \\ \eta \end{matrix} \right\} = \frac{1}{\Delta} \left[\begin{matrix} (y_3 - y_1) & -(x_3 - x_1) \\ -(y_2 - y_1) & (x_2 - x_1) \end{matrix} \right] \left\{ \begin{matrix} x - x_1 \\ y - y_1 \end{matrix} \right\} \tag{3.27}$$

where, $\Delta = (x_2 - x_1)(y_3 - y_1) - (x_3 - x_1)(y_2 - y_1)$

Hence,

$$\begin{aligned} \frac{\partial \xi}{\partial x} &= \frac{y_3 - y_1}{\Delta} & \frac{\partial \xi}{\partial y} &= -\frac{x_3 - x_1}{\Delta} \\ \frac{\partial \eta}{\partial x} &= -\frac{y_2 - y_1}{\Delta} & \frac{\partial \eta}{\partial y} &= \frac{x_2 - x_1}{\Delta} \end{aligned} \tag{3.28}$$

Transforming $dxdy$ into $d\xi d\eta$:

Let the differential area $dxdy$ is formed through vectors $\hat{dx}$ and $\hat{dy}$ with magnitude dA and direction normal to the elemental area is $\hat{k}$

$$dA = dx\,dy = [\hat{dx} \times \hat{dy}] \cdot \hat{k} \tag{3.29}$$

$$\begin{aligned} dx\,dy &= [\,(\,\tfrac{\partial x}{\partial \xi}\,d\xi\,\hat{i} + \tfrac{\partial x}{\partial \eta}\,d\eta\,\hat{j}\,) \times (\,\tfrac{\partial y}{\partial \xi}\,d\xi\,\hat{i} + \tfrac{\partial y}{\partial \eta}\,d\eta\,\hat{j}\,)\,]\cdot \hat{k} \\ &= [\,\tfrac{\partial x}{\partial \xi} \cdot \tfrac{\partial y}{\partial \eta} - \tfrac{\partial x}{\partial \eta} \cdot \tfrac{\partial y}{\partial \xi}\,]\,d\xi\,d\eta \\ &= |J|\,d\xi\,d\eta \end{aligned} \tag{3.30}$$

or the Jacobian matrix is given by

$$J = \begin{bmatrix} \frac{\partial x}{\partial \xi} & \frac{\partial y}{\partial \xi} \\ \frac{\partial x}{\partial \eta} & \frac{\partial y}{\partial \eta} \end{bmatrix} \tag{3.31}$$

Substituting from equation (3.5)

$$|J| = (x_2 - x_1)\,(y_3 - y_1) - (x_3 - x_1)\,(y_2 - y_1) \tag{3.32}$$

Hence $\int_e f\,(x,y)\,dx\,dy$ may be written as

$$\int_e f\,(x,y)\,dx\,dy = \int_{e_m} \hat{f}\,(\xi,\eta)\,d\xi\,d\eta \tag{3.33}$$

such that $\hat{f}\,(\xi,\eta)\,d\xi\,d\eta = |J|\,f\,(x(\xi,\eta), y(\xi,\eta))$.

Numerical Integration:

To compute $\int_{A_m} \hat{f}\,(\xi,\eta)\,d\xi\,d\eta$ *Gaussian quadrature* for two-dimentional integrals is used through which

$$\int_{A_m} \hat{f}\,(\xi,\eta)\,d\xi\,d\eta \approx \sum_{i=1}^{n} \hat{f}\,(\,\xi_i,\eta_i\,)\,w_i\,|J| \tag{3.34}$$

where, n is the number of quadrature points, w_i is the weight at quadrature point (ξ_i, η_i) and the Jacobian $|J|$ is the area of the element e.

Order of numerical integration is greater than or equal to $(p+1)/2$ where, p is the order of the integrand.

Shape Function Derivatives:

Shape functions are defined in the master element i.e. $N_i = N_i(\xi, \eta)$. Its derivatives with respect to x and y can be given as

$$\begin{aligned} N_{i,x} &= \frac{\partial N_i}{\partial \xi} \cdot \frac{\partial \xi}{\partial x} + \frac{\partial N_i}{\partial \eta} \cdot \frac{\partial \eta}{\partial x} \\ N_{i,y} &= \frac{\partial N_i}{\partial \xi} \cdot \frac{\partial \xi}{\partial y} + \frac{\partial N_i}{\partial \eta} \cdot \frac{\partial \eta}{\partial y} \end{aligned} \tag{3.35}$$

Since shape functions are defined in terms of normalised coordinates ξ and η the terms $\frac{\partial N_i}{\partial \xi}$ and $\frac{\partial N_i}{\partial \eta}$ can be evaluated at any point in the domain.

3.5.2 CURVED ELEMENTS

The cut-out profile is represented in terms of a curved edge. Thus, at a cut-out edge, linear mapping will be inadequate unless a very fine mesh is employed at the cut-out. Further, for higher order approximations (i.e. $p \geq 2$), significant errors in the solution quantities can be obtained for the elements at the cut-out, if proper geometric transformations are not employed. Special care has to be taken at the curved boundaries, to ensure that the errors due to geometric approximations do not become significant.

3.5.3 MAPPING CURVED ELEMENTS

For elements with curved edges, a quadratic blending function type mapping is employed. The mapping can be given as:

$$\begin{aligned} X &= x_1 N_1 + x_2 N_2 + x_3 N_3 + \alpha N_{i+3} \\ Y &= y_1 N_1 + y_2 N_2 + y_3 N_3 + \beta N_{i+3} \end{aligned} \tag{3.36}$$

where α, β are suitable coefficients; $i = 1, 2, 3$ is the curved edge. Below, we describe how α and β are obtained.

Let us, for example, consider the curved edge to be a segment of an ellipse. For any

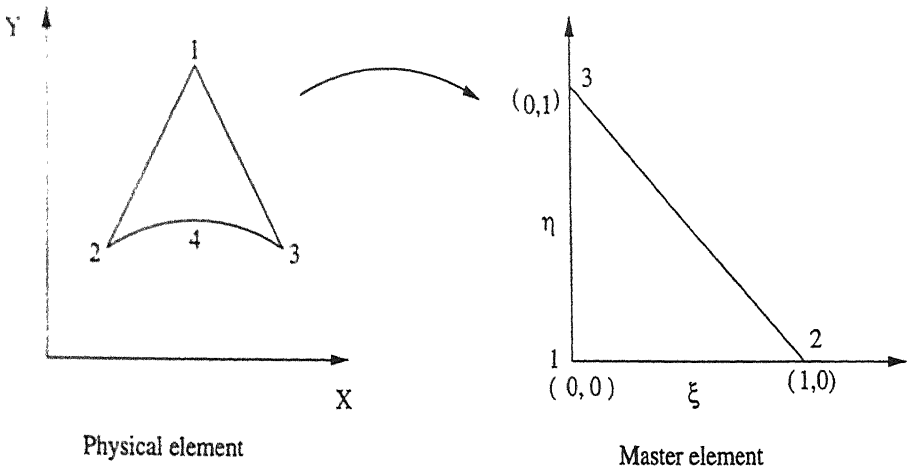

Figure 3.3: Curved element mapping

point on the ellipse we have the relations

$$\begin{aligned} x^* &= a\,\cos\theta \\ y^* &= b\,\sin\theta \end{aligned} \tag{3.37}$$

The curve between two nodes is approximated by using the quadratic shape functions. Thus, we have

$$\begin{aligned} \bar{x} &= x_1\,N_1(\xi) + x_2\,N_2(\xi)\; + \alpha\,N_3(\xi) \\ \bar{y} &= y_1\,N_1(\xi) + y_2\,N_2(\xi)\; + \beta\,N_3(\xi) \end{aligned} \tag{3.38}$$

where

$$N_1(\xi) = \tfrac{1-\xi}{2};\quad N_2(\xi) = \tfrac{1+\xi}{2};\quad N_3(\xi) = -\sqrt{6}\,(1-\xi^2) \tag{3.39}$$

are the one-dimensional hierarchic shape functions defined on the curved edge.

Let us further define the following functional on the edge:

$$J = \int_{-1}^{1} (\,\bar{x} - x^*\,)^2\,d\xi \tag{3.40}$$

α is the minimiser of J. Thus α can be obtained from

$$\tfrac{\partial J}{\partial \alpha} = \int_{-1}^{1} (\,\bar{x} - x^*\,)\,N_3(\xi)\,d\xi = 0$$

Hence,

$$\alpha \int_{-1}^{1} N_3(\xi)^2 = \int_{-1}^{1} (\,x^* - \bar{x}\,)\,N_3\,d\xi \tag{3.41}$$

$$\alpha = \frac{\int_{-1}^{1} (x^* - \bar{x})\, N_3\, d\xi}{\int_{-1}^{1} N_3^2\, d\xi} \tag{3.42}$$

Similarly, we can find β, by defining $J = \int_{-1}^{1} (\bar{y} - y^*)\, d\xi$ and β as minimiser.

3.6 BOUNDARY CONDITIONS

From the variational formulation of the problem several combinations of the applicable boundary conditions in terms of forces/displacements, moments/rotations, higher moments/curvatures are possible. However, for simplicity, we list certain typical boundary conditions (considered in this study) below.

1. Point support boundary condition
2. Simply supported boundary condition
3. Clamped edge boundary condition
4. Symmetry edge boundary condition
5. Free edge (all traction components are zero).

While applying boundary conditions we look at those degrees of freedom which are to be set zero (see Table (3.1) and Table (3.2)).

Point Supported	Simply Supported	Clamped Edge	Symmetry Line
$w_0 = 0$	$w_0 = 0$	$w_0 = 0$	$v_0 = 0$
	$u_0 = \theta_x = \psi_x = 0$	$u_0 = \theta_x = \psi_x = 0$	$\theta_y = \psi_y = 0$
		$v_0 = \theta_y = \psi_y = 0$	

Table 3.1: Typical boundary conditions on x edge (y = constant)

Point Supported	Simply Supported	Clamped Edge	Symmetry Line
$w_0 = 0$	$w_0 = 0$	$w_0 = 0$	$u_0 = 0$
	$v_0 = \theta_y = \psi_y = 0$	$u_0 = \theta_x = \psi_x = 0$	$\theta_x = \psi_x = 0$
		$v_0 = \theta_y = \psi_y = 0$	

Table 3.2: Typical boundary conditions on y edge (x = constant)

Solving the finite element problem for the seven DOFS, we can obtain the approximate values of displacements, strains and stresses at any point in a lamina. However, a-priori we have no knowledge of the accuracy of the solution quantities. A good approximation of the stress components is essential to accurately find the first-ply failure criterion. In the next section, we outline a simple procedure for the a-posteriori recovery of a "better" stress field from the finite element solution.

Chapter 4

A-POSTERIORI RECOVERY OF POINTWISE STRESSES AND ERROR ESTIMATION

4.1 INTRODUCTION

In a typical engineering analysis a *mathematical* model for physical problem is first selected, such that it incorporates the essential features of the actual physical problem. The finite element method determines an approximation to the exact solution of the mathematecal model. The computed solution should be compared with exact solution of the mathematical model which is being solved. Hence, the computed results can be used to make engineering decisions only when one can guarantee that finite element solution is sufficiently close to the exact solution of the mathematical model problem. In general, the results of interest obtained from the finite element solution can be very different from those corresponding to the exact solution of the mathematical formulation and can lead to serious design errors. Thus, it is imperative to accompany any computational analysis with an accurate indication of the error in the quantity of interest.

The error estimator should be reliable. Unreliable error estimates are dangerous because they could lead to a misleading confidence in the computed quantities. The reliability of the error estimator has to be understood with respect to the solution quantity of interest. Here, the error estimator is constructed for the energy norm of the error and it is assumed that if the error in the global energy norm is low then all solution quantities of interest are also reasonably accurate.

In this study a simple procedure for the recovery of strains, from the finite element solution, using patchwise data is proposed (as an extension of the method in [20]). This recovered strain will be used to design a simple error estimator.

4.2 PROCEDURE

The idea behind the error estimation of laminated plate is that, the in-plane strains (the recovered one) are assumed to be of order p whereas the transverse shear strains are an order higher i.e. $(p+1)$ and they are of the same mathematical form as that for the exact solution of the model as in Eq. (2.5) and are given as:

$$\begin{aligned}
\epsilon^*{}_{xx} &= \epsilon^{*0}_{xx} + z\,\epsilon^{*1}_{xx} + z^3\,\epsilon^{*2}_{xx} \\
\epsilon^*{}_{yy} &= \epsilon^{*0}_{yy} + z\,\epsilon^{*1}_{yy} + z^3\,\epsilon^{*2}_{yy} \\
\gamma^*{}_{xy} &= \gamma^{*0}_{xy} + z\,\gamma^{*1}_{xx} + z^3\,\gamma^{*2}_{xy} \\
\gamma^*{}_{yz} &= \gamma^{*0}_{yz} + z^2\,\gamma^{*1}_{yz} \\
\gamma^*{}_{xz} &= \gamma^{*0}_{xz} + z^2\,\gamma^{*1}_{xz}
\end{aligned} \tag{4.1}$$

In-plane strains of the strain tensor are approximated by p^{th} order polynomial.

e.g.

$$\epsilon^{*0}_{xx} = \sum_{i=1}^{(p+1)(p+2)/2} e^{*0}_{xx,i}\, q_i \tag{4.2}$$

Similarly, $\epsilon^{*1}_{xx}, \epsilon^{*2}_{xx}, \epsilon^{*0}_{yy}, \epsilon^{*1}_{yy}, \epsilon^{*2}_{yy}, \epsilon^{*0}_{xy}, \epsilon^{*1}_{xy}, \epsilon^{*2}_{xy}$ strain components can be approximated as above.

And, transverse shear strains of the strain tensor are approximated by $(p+1)^{th}$ order polynomial.

e.g.

$$\gamma^{*0}_{yz} = \sum_{i=1}^{(p+2)(p+3)/2} e^{*0}_{yz,i}\, q_i \tag{4.3}$$

Similarly, $\gamma^{*1}_{yz}, \gamma^{*0}_{xz}, \gamma^{*1}_{xz}$ strain components can be approximated as above.

where q_i are *monomials* (defined in terms of a local coordinate system described later).

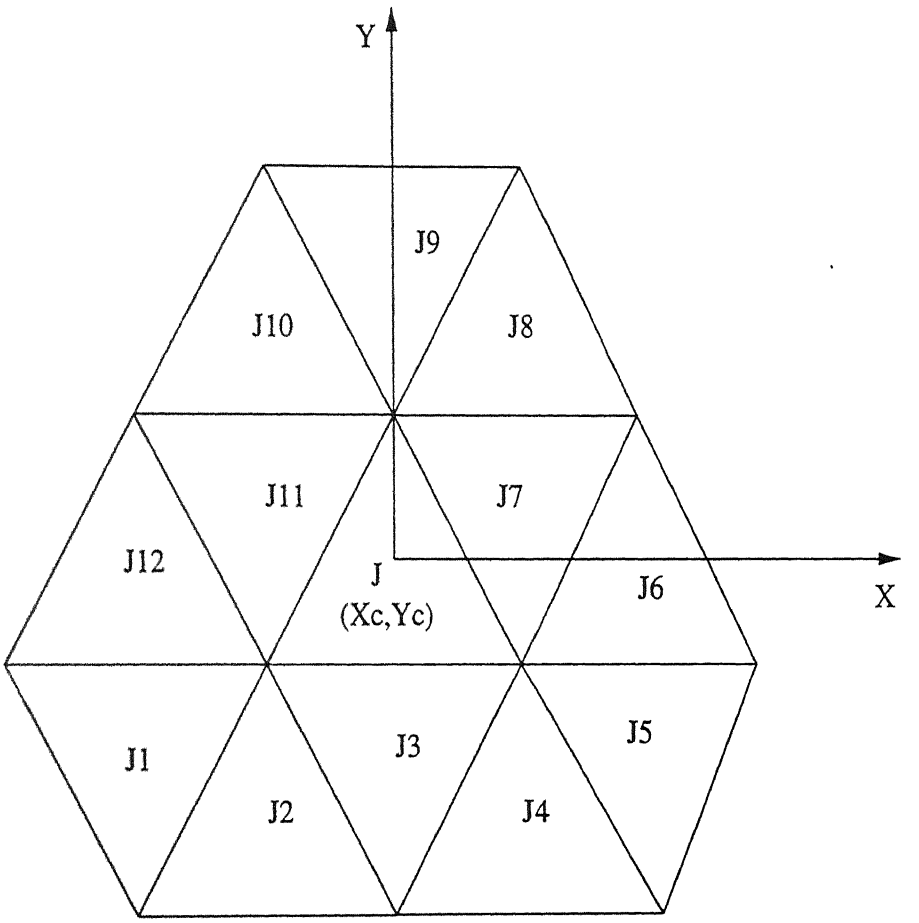

Figure 4.1: Patch over element J

A patch is constructed by taking element J and one layer of elements around it, as shown in fig. (4.1). Let the centroid of element J is (X_c, Y_c).

A local coordinate system can be defined with X_c, Y_c as the centre as:

$$\begin{Bmatrix} \hat{x} \\ \hat{y} \end{Bmatrix} = \begin{Bmatrix} x - X_c \\ y - Y_c \end{Bmatrix} \tag{4.4}$$

The monomials q_i are given as,

$$\begin{aligned}
q_1 &= 1 & q_2 &= \hat{x} & q_3 &= \hat{y} \\
q_4 &= \hat{x}^2 & q_5 &= \hat{x}\hat{y} & q_6 &= \hat{y}^2 \\
q_7 &= \hat{x}^3 & q_8 &= \hat{x}^2\hat{y} & q_9 &= \hat{x}\hat{y}^2 \\
q_{10} &= \hat{y}^3 & q_{11} &= \hat{x}^4 & q_{12} &= \hat{x}^3\hat{y} \\
q_{13} &= \hat{x}^2\hat{y}^2 & q_{14} &= \hat{x}\hat{y}^3 & q_{15} &= \hat{y}^4 \\
q_{16} &= \hat{x}^5 & q_{17} &= \hat{x}^4\hat{y} & q_{18} &= \hat{x}^3\hat{y}^2 \\
q_{19} &= \hat{x}^2\hat{y}^3 & q_{20} &= \hat{x}\hat{y}^4 & q_{21} &= \hat{y}^5
\end{aligned} \tag{4.5}$$

Now to recover a smoothened strain field we should find smoothened strain components, that is, 9 $[(p+1)(p+2)/2]$ + 4 $[(p+2)(p+3)/2]$ unknown coefficients. To get these coefficients, as aforesaid, the strain recovery procedure uses the principle of minimization of energy norm of error i.e. the energy due to errors in strain and stress components, over the patch considered. A typical patch over element J is shown in fig. (4.1). In this, the strain components of the finite element solution are known. The material properties and other relavent information about patch is available. From this, the strain energy of the error can be computed as,

$$J = \frac{1}{2} \int_{A_{patch}} \int_{z=-\frac{h}{2}}^{\frac{h}{2}} (\underline{\epsilon}_{FE} - \underline{\epsilon}^*) \cdot \bar{Q} \, (\underline{\epsilon}_{FE} - \underline{\epsilon}^*) \, dz \, dA \tag{4.6}$$

where $\underline{\epsilon}^*$ and $\underline{\epsilon}_{FE}$ are recovered and finite element strain vectors and $\bar{Q}$ is material stiffness matrix, respectively.

The minimization of this function with respect to each unknown coefficient of recovered strain term gives 9 $[(p+1)(p+2)/2]$ + 4 $[(p+2)(p+3)/2]$ equations. Solution of this system of equation gives the unknown coefficients. Using these coefficients smoothened strain components are constructed over the patch.

The above step is followed by *Re-construction.* In this, the in-plane stresses are constructed using material properties i.e. from constitutive equation. Although,

the recovered shear strains are improved over the finite element strains, equilibrium equations are used to get the transverse stress field as the model will not give good transverse stress components (because strain continuity has been assumed).

The strain energy from recovered and finite element strains are calculated over the whole domain.

$$\begin{aligned} U_{recov} &= \tfrac{1}{2} \textstyle\sum_{j=1}^{N} \int_j \underline{\sigma}^* \cdot \underline{\epsilon}^* \, dV_{patch} \\ U_{fem} &= \tfrac{1}{2} \textstyle\sum_{j=1}^{N} \int_j \underline{\sigma}_{fe} \cdot \underline{\epsilon}_{fe} \, dV_{patch} \end{aligned} \tag{4.7}$$

where U_{recov} and U_{fem} are the strain energies over the whole domain from recovered strains and finite element strains, respectively, $\underline{\sigma}^*$ and $\underline{\sigma}_{fe}$ are recovered and finite element stresses, $\underline{\epsilon}^*$ and $\underline{\epsilon}_{fe}$ are the recovered and finite element strains and N is the number of elements in the domain.

The energy norm ε of the error is calculated as:

$$\varepsilon = \sqrt{2\, U(\underline{u}^* - \underline{u}_{fe})} \tag{4.8}$$

4.3 ADAPTIVITY

The energy norm of the error obtained using the recovered stress field is used to refine the mesh. The procedure involves the computation of the energy norm of the error in each element, followed by a ranking of the elements in the order of highest contributions to the total error. The elements contributing eighty percent of the maximum error are refined. This procedure is repeated till convergence to within the specified tolerances is obtained. It should be noted that adaptive analysis requires repeated solution of the boundary value problem, with the modified meshes. Thus, the cost of computation increases (see [20] for details).

Chapter 5

DESCRIPTION OF OPTIMIZATION PROBLEM

The plate with dimensions of X, Y and a centrally located cut-out of elliptical shape with initial size $2a, 2b$ and its rotation θ, is shown in fig.(5.1). Here, $2a$ is major axis, $2b$ is minor axis.

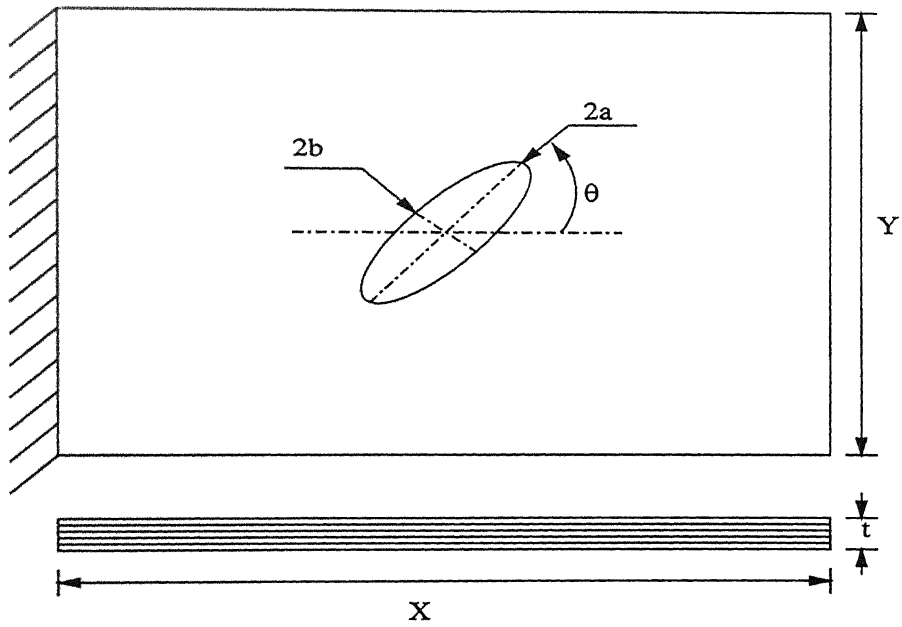

Figure 5.1: Initial shape of plate and cut-out

The objective of the optimization probem is to minimize the weight of the plate. Since all the laminae of same material are taken, the objective becomes the minimization of the plate material area. Hence, the design parameters are, semi-major axis - a, semi-minor axis - b.

Objective function: Minimize W

Or Minimize Area of the material $A = X\,Y - \pi\,a\,b$

Subject to Stress state $\leq$ 0.8(Tsai Wu failure criterion).

$\frac{Y}{8} < a, b < 0.4\ Y$

5.1 OPTIMIZATION TECHNIQUE

Complex Search Method algorithm is used for solving this optimization problem [21].

The algorithm begins with a number of feasible points created at random. If a point is found to be infeasible, a new point is created using previously-generated points. Usually, the infeasible point is pushed towards the centroid of the previously- found feasible points. Once a set of feasible points is found, the worst point is reflected about the centroid of rest of the points to find a new point. Depending on the feasibility and function value of the new point, the point is further modified or accepted. If the new point falls outside the variable boundaries, the point is modified to fall on the violated boundary. If new point is infeasible, the point is retracted towards the feasible points. The worst point in the simplex is replaced by this new feasible point and algorithm continues for next iteration.

Here, the reflection parameter used is 1.3 and convergence parameter is 0.01.

5.2 FAILURE CRITERIA

5.2.1 TSAI-WU FAILURE CRITERION

The failure criterion based on interactive failure theories is considered. We have used here second-order tensor polynomial criterion proposed by Tsai-Wu [22]. It is a complete quadratic tensor polynomial with the linear terms included. The most compact form for expressing this theory is through tensor notation:

$$F_i\,\sigma_i + F_{ij}\,\sigma_i\,\sigma_j \leq 0.8 \quad i,j = 1,2,....6 \tag{5.1}$$

where F_i and F_{ij} are the strengths tensors established through experimental procedures and are related to failure strengths in principal lamina directions. Here, right hand side of above equation is deliberately taken 0.8 instead of 1 as a safe constraint for the optimization problem mentioned earlier. For orthotropic lamina this reduces to: (see [27], [28])

$$\begin{aligned} &F_1\sigma_1 + F_2\sigma_2 + F_6\sigma_6 + F_{11}\sigma_1^2 + F_{22}\sigma_2^2 + F_{33}\sigma_3^2 + F_{44}\sigma_4^2 \\ &+F_{55}\sigma_5^2 + F_{66}\sigma_6^2 + 2F_{12}\sigma_1\sigma_2 + 2F_{16}\sigma_1\sigma_6 + 2F_{26}\sigma_2\sigma_6 \leq 0.8 \end{aligned} \tag{5.2}$$

and for plane stress this reduces to:

$$\begin{aligned} &F_1\sigma_1 + F_2\sigma_2 + F_6\sigma_6 + F_{11}\sigma_1^2 + F_{22}\sigma_2^2 + F_{66}\sigma_6^2 \\ &+2F_{12}\sigma_1\sigma_2 + 2F_{16}\sigma_1\sigma_6 + 2F_{26}\sigma_2\sigma_6 \leq 0.8 \end{aligned} \tag{5.3}$$

The strength tensors are given below:

$$\begin{aligned} &F_1 = \tfrac{1}{X_T} - \tfrac{1}{X_C}, && F_2 = \tfrac{1}{Y_T} - \tfrac{1}{Y_C}, && F_3 = \tfrac{1}{Z_T} - \tfrac{1}{Z_C}, \\ &F_{11} = \tfrac{1}{X_T X_C}, && F_{22} = \tfrac{1}{Y_T Y_C}, && F_{33} = \tfrac{1}{Z_T Z_C}, \\ &F_{44} = \tfrac{1}{R^2}, && F_{55} = \tfrac{1}{S^2}, && F_{66} = \tfrac{1}{T^2}, \\ &F_{12} = -\tfrac{1}{2}\tfrac{1}{\sqrt{X_T X_C Y_T Y_C}}, && F_{13} = -\tfrac{1}{2}\tfrac{1}{\sqrt{X_T X_C Z_T Z_C}}, && F_{23} = -\tfrac{1}{2}\tfrac{1}{\sqrt{Y_T Y_C Z_T Z_C}} \end{aligned} \tag{5.4}$$

where subscript T denotes tensile strengths, C denotes compressive strengths. X, Y and Z are the strengths in L, T and T' directions, respectively. R, S, T are shear strengths in TT', LT' and LT planes, respectively. T' is pependicular to plane LT. (see fig. 2.2).

5.2.2 PROCEDURE FOR FIRST-PLY FAILURE ANALYSIS

The first-ply failure analysis is based on the assumption that a given ply would fail if the failure index at any point within the ply reaches a value of unity. The failure index is defined as '$F_i\,\sigma_i + F_{ij}\,\sigma_i\,\sigma j$'. The steps used in the iterative procedure are listed here:

Step 1 Find the displacement field for a small initial load.

Step 2 Find the stresses for the above displacement field.

Step 3 Transform the stresses into the material coordinates.

Step 4 Find the maximum failure index.

Step 5 Check whether the laminate has failed or not.

Step 6 If not, increase or decrease the initial load appropriately.

Step 7 Repeat the steps 1 to 6 until the laminate fails.

The maximum failure index is determined by carrying out a sequential search at certain preselected points within the laminate. The sequence of search is as follows:

1. Consider the first element of the finite element mesh.
2. Consider the first Gaussian point within the element.
3. Consider the first ply (from top) of the laminate.
4. Consider the top of the current ply.
5. Find the failure index at that location.
6. Check whether this is greater than the previous value.
7. If yes, store the element number, Gaussian point number, ply number, location on the ply and failure index and go to the next location (middle of the ply, bottom of the ply, etc).
8. If answer in Step 6 is no, then do not store the failure data, but go to the next location and repeat Steps 5-8.
9. Go to the next ply.

10. Go to the next Gaussian point.
11. Go to next element.
12. Continue the search until all the elements in the finite element mesh are searched for the maximum failure index.

Chapter 6

NUMERICAL RESULTS AND DISCUSSION

The shape optimization process requires computation of constraint information (e.g. first-ply failure criterion). In order to guarantee the reliability of the constraint information, the accuracy of the plate model (and its implementation), the discretisation procedure and postprocessing module have to be established. In this chapter, a detailed validation study for the plate model, along with the influence of mesh refinement and p - inrichment, is done. This is followed by the shape optimization problem with and without adaptivity.

6.1 VALIDATION OF PLATE MODEL

In this section, first we define the problem for validation study. It is followed by validation study for *Thin, Moderately thick,* and *Thick plates.* Lastly, validation for *first-ply failure load* of laminates is presented.

Remark 1: The definition thin, moderately thick and thick plates depends upon length to thickness ($\frac{X}{h}$) ratio, loadings, boundary conditions etc. Here, we have defined them roughly.

Remark 2: Unless specified, the analysis is done for full plate.

6.1.1 PROBLEM DEFINITION

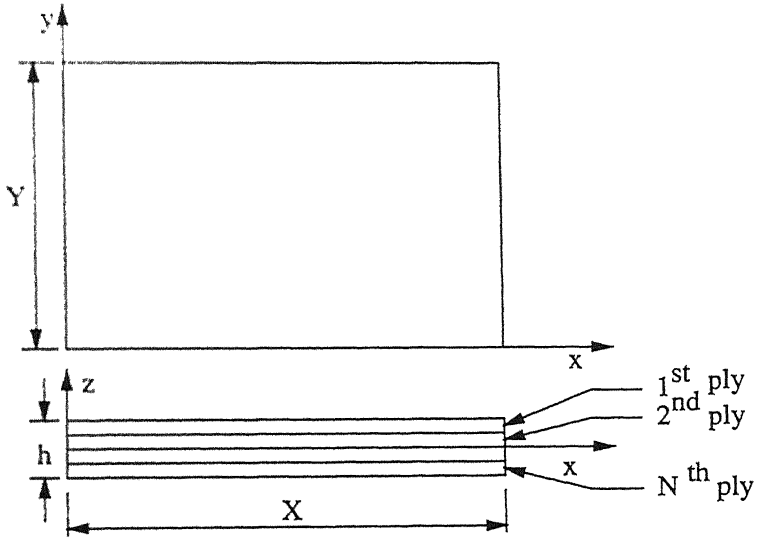

Figure 6.1: Problem plate for plate model validation

A laminated plate of the dimensions shown in fig. (6.1) has been considered for analysis.

The plate is loaded transversely on the upper surface through the sinusoidal load:

$$q_z(x,y) = -q_c \sin(\frac{m\,\pi\,x}{X}) \sin(\frac{n\,\pi\,y}{Y}) \tag{6.1}$$

or with uniformly distributed transverse load:

$$q_z(x,y) = -q_0 \tag{6.2}$$

The transverse mid-plane displacement at the centre of the plate, w_0 (unless specified) is normalised as $\bar{w}_0$:

$$\bar{w}_0 = w_0 \frac{E_2\,h^3}{q_c\,a^4}\,10^2$$

When load is uniformly distributed transvese load, the term q_c is replaced by q_0.

Unless specified in all problems the mesh types used are shown in fig. (6.2).

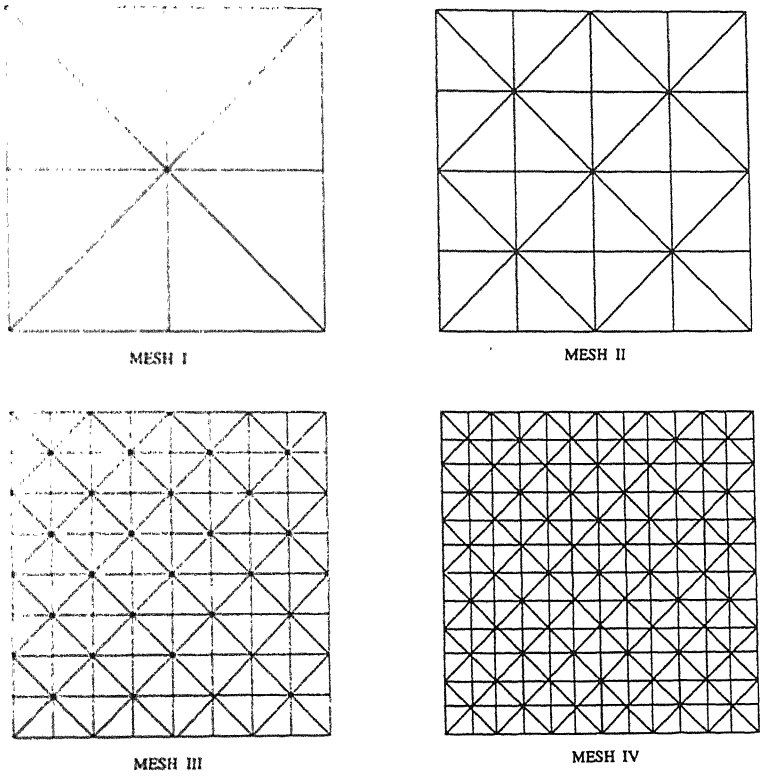

Figure 6.2: Mesh patterns used for plate validation study

6.1.2 THICK PLATES

The plates with X/h ratio upto 8 are treated as thick plates.

PROBLEM 1

A three layer simply supported square laminated plate under sinusoidal transverse load is analysed. The lamina properties are as follows:

$\frac{E_1}{E_2} = 25; \quad E_2 = E_3 = 6.89 \times 10^3 N/mm^2;$

$\frac{G_{23}}{E_2} = 0.2; \quad \frac{G_{13}}{E_2} = \frac{G_{12}}{E_2} = 0.5;$

$\nu_{12} = \nu_{23} = \nu_{13} = 0.25;$

$X = 25.4\, mm; \quad \frac{X}{h} = 4;$

Thickness of each layer $= \frac{h}{3}$; Fibre orientations $= [0°/90°/0°]$;

$q_c = 6.89 \times 10^{-3} N/mm^2$; m = 1 ; n = 1

Results of this problem are tabulated in table 6.1, 6.2.

Mesh Type	$\bar{w}_0$	$\Pi_p \times 10^{-5}$
Mesh I	-1.9230	-1.7371
Mesh II	-1.9242	-1.7395
Mesh III	-1.9258	-1.7397
Mesh IV	-1.9260	-1.7397
Kant et al [16]	-1.9058	-

Table 6.1: Validation study for thick plate with mesh refinement and $p = 3$

p	$\bar{w}_0$	$\Pi_p \times 10^{-5}$
1	-1.8339	-1.6009
2	-1.9267	-1.7388
3	-1.9258	-1.7397
4	-1.9261	-1.7397
Kant et al [16]	-1.9058	-

Table 6.2: Validation study for thick plate with p refinement for Mesh III

We can see from above results (see table (6.1), (6.2)) that:

- The results from our study are close to the one with reference results osbtained by Kant et al [16].
- For p=3 the effect of mesh refinement shows that results converge with mesh refinement above III.
- And with p refinement it converges for $p \geq 3$.
- The reference results are for a fixed rectangular mesh with four elements and with no convergence analysis. Hence, we see difference in the the two results. The total potential converges to a value of -1.7397×10^{-5}.

PROBLEM 2

A rectangular laminated plate simply supported along all edges and subjected to transverse sinusoidal loading is analysed. The laminae properties are listed as follows:

$E_1 = 138\ N/mm^2$; $E_2 = 9.3\ N/mm^2$;

$G_{12} = G_{21} = 4.6\ N/mm^2$; $G_{13} = 3.1\ N/mm^2$;

$\nu_{12} = 0.3$; $\nu_{13} = \nu_{23} = 0.5$;

$X = 5\ mm$; $Y = 3.5\ mm$; $h = 1\ mm$;

Thickness of each layer $= \frac{h}{4}$; Lamination scheme $[0/90]_s$;

$q_c = 1\ N/mm^2$; m = 1; n = 1

The results are analysed for quarter plate with mesh shown in fig. (6.3) and are tabulated in table 6.3 through 6.6.

Mesh Type	$w_0 \times 10^{-4}$	$\Pi_p \times 10^{-4}$
Mesh I	-5.8090	-3.1683
Mesh II	-5.8439	-3.1954
Mesh III	-5.8467	-3.1974
Mesh IV	-5.8468	-3.1975
3-D solid [19]	-5.7363	-3.0851

Table 6.3: Validation study for thick plate with mesh refinement for $p = 2$

p	$w_0 \times 10^{-4}$	$\Pi_p \times 10^{-4}$
1	-5.2480	-2.8603
2	-5.8439	-3.1954
3	-5.8467	-3.1975
4	-5.8469	-3.1975
3-D solid [19]	-5.7363	-3.0851

Table 6.4: Validation study for thick plate with p refinement for Mesh II

Mesh Type	σ^*_x $(\frac{a}{2}, \frac{b}{2}, -\frac{h}{2})$	σ^*_y $(\frac{a}{2}, \frac{b}{2}, -\frac{h}{2})$	τ^*_{xy} $(a, b, -\frac{h}{2})$	σ_x $(\frac{a}{2}, \frac{b}{2}, -\frac{h}{2})$	σ_y $(\frac{a}{2}, \frac{b}{2}, -\frac{h}{2})$	τ_{xy} $(a, b, -\frac{h}{2})$
Mesh I	8.5821	1.8848	-0.9662	8.0526	1.7647	-0.8916
Mesh II	7.9947	1.7597	-0.9057	7.9523	1.7496	-0.8990
Mesh III	7.9137	1.7410	-0.8989	7.9118	1.7403	-0.8982
Mesh IV	7.9042	1.7384	-0.8980	7.9042	1.7382	-0.8970
3-D solid [19]	7.7388	1.9267	-0.8602	7.7388	1.9267	-0.8602

Table 6.5: Comparison of stresses with mesh refinement for $p = 2$

p	σ^*_x $(\frac{a}{2}, \frac{b}{2}, -\frac{h}{2})$	σ^*_y $(\frac{a}{2}, \frac{b}{2}, -\frac{h}{2})$	τ^*_{xy} $(a, b, -\frac{h}{2})$	σ_x $(\frac{a}{2}, \frac{b}{2}, -\frac{h}{2})$	σ_y $(\frac{a}{2}, \frac{b}{2}, -\frac{h}{2})$	τ_{xy} $(a, b, -\frac{h}{2})$
1	7.1042	1.5524	-0.8073	6.9450	1.5100	-0.7813
2	7.9947	1.7597	-0.9057	7.9523	1.7496	-0.8990
3	7.8687	1.7298	-0.8936	7.8972	1.7363	-0.8970
4	7.8663	1.7513	-0.8980	7.8980	1.7365	-0.8972
3-D solid [19]	7.7388	1.9267	-0.8602	7.7388	1.9267	-0.8602

Table 6.6: Comparison of stresses with p refinement for Mesh II

In the above tables 6.5, 6.6 $\sigma^*_x, \sigma^*_y, \tau^*_{xy}$ denotes recovered stresses and $\sigma_x, \sigma_y, \tau_{xy}$ denotes finite element stresses.

From above results we observe that:

- The results converge for mesh refinement above III.
- With p refinement for mesh III results converge for $p \geq 3$.
- The plate model considered shows the total potential values higher than the reference values. This difference between total potential values is because the plate model considered here assumes a smooth strain field through the thickness, which leads to a jump in the values of the transverse stresses at the interfaces. This is in direct violation of the stress continuity requirement (from 3-D solid elasticity) at the interface.

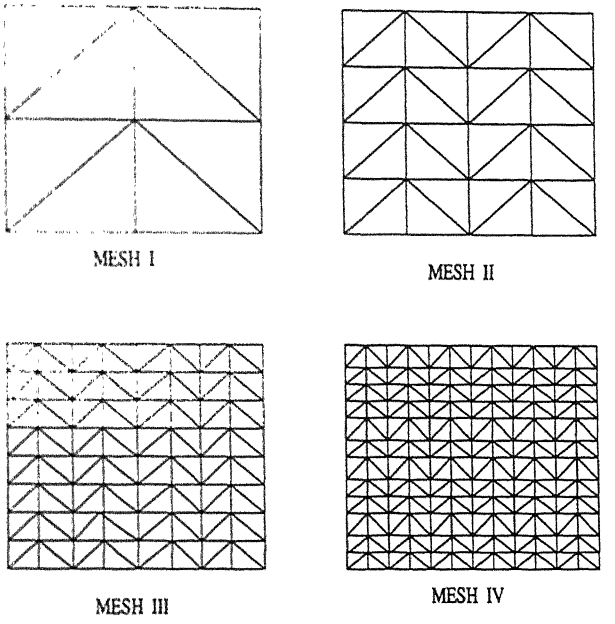

Figure 6.3: Mesh patterns used for plate validation study

6.1.3 MODERATELY THICK PLATES

The plates with X/h ratio between 8 to 15 are treated as moderately thick plates.

PROBLEM 3

The problem description is same as problem 1 with the change $\frac{X}{h} = 10$.

Results are tabulated in table 6.7, 6.8.

Mesh Type	$\bar{w}_0$	$\Pi_p \times 10^{-4}$
Mesh I	-0.7174	-1.0098
Mesh II	-0.7171	-1.0127
Mesh III	-0.7176	-1.0129
Mesh IV	-0.7176	-1.0129
Kant et al [16]	-0.7164	-

Table 6.7: Validation study for moderately thick plate with mesh refinement for $p = 3$

p	$\bar{w}_0$	$\Pi_p \times 10^{-4}$
1	-0.6202	-0.8459
2	-0.7175	-1.0118
3	-0.7176	-1.0129
4	-0.7176	-1.0129
Kant et al [16]	-0.7164	-

Table 6.8: Validation study for moderately thick plate with p refinement for Mesh III

The observations for this study show that:

- The displacement show convergence to a value of -0.7176 and total potential -1.0129×10^{-4} for III and higher levels of mesh refinement.
- For a mesh with III refinements, the convergence is observed for $p \geq 3$.

- The difference in the displacement is because in the reference study a fixed mesh was used for analysis and no convergence study was done.

PROBLEM 4

Four-layer antisymmetric angle-ply square plate subjected to uniformly distributed transverse load is analysed for following boundary conditions:

1. Simply supported (SS)
2. Clamped edges (CC)

The laminae properties are:

$\frac{E_1}{E_2} = 10; \quad E_2 = 6.89 \times 10^3 N/mm^2;$

$G_{12} = G_{13} = 0.6\, E_2; \quad G_{23} = 0.5\, E_2;$

$\nu_{12} = \nu_{13} = \nu_{23} = 0.25;$

$X = 25.4\, mm; \quad \frac{X}{h} = 10;$

Thickness of each layer $= \frac{h}{4}$; Ply-orientations $[45°/-45°/45°/-45°]$;

$q_0 = 6.89 \times 10^{-3} N/mm^2$.

The results are tabulated in table 6.9, 6.10.

The observations from our study show that:

- Both non-dimensionalised displacement and total potential converges for mesh refinements above level III.
- For a fixed level of refinement III, the convergence with p refinement can be seen for $p \geq 3$.
- The displacements from our study are higher than those obtained by Reddy and Miravete [29]. We have used HSDT model while they have used CLPT and solved the problem by Levy method with state-space approach.
  The HSDT model leads to a more flexible structure as compared to the CLPT model.

Boundary Condition	Mesh Type	$\bar{w}_0$	$\Pi_p \times 10^{-4}$
S S	Mesh I	-1.1062	-2.6566
	Mesh II	-1.1059	-2.6682
	Mesh III	-1.1068	-2.6698
	Mesh IV	-1.1069	-2.6700
	Reddy and Miravete [29]	-1.0000	-
C C	Mesh I	-0.5562	-1.1342
	Mesh II	-0.5779	-1.1756
	Mesh III	-0.5799	-1.1819
	Mesh IV	-0.5800	-1.1812
	Reddy and Miravete [29]	-0.5578	-

Table 6.9: Validation study for moderately thick plate with mesh refinement for $p = 3$

Boundary Condition	p	$\bar{w}_0$	$\Pi_p \times 10^{-4}$
S S	1	-0.8862	-2.0615
	2	-1.1055	-2.6642
	3	-1.1068	-2.6698
	4	-1.1069	-2.6700
	Reddy and Miravete [29]	-1.0000	-
C C	1	-0.4632	-0.9143
	2	-0.5773	-1.1719
	3	-0.5799	-1.1819
	4	-0.5801	-1.1812
	Reddy and Miravete [29]	-0.5578	-

Table 6.10: Validation study for moderately thick plate with p refinement for Mesh III

6.1.4 THIN PLATES

Plates with ratio $\frac{X}{h}$ above 15 are treated to be thin plates.

PROBLEM 5

The problem description is same as in problem 1 with the change that $\frac{X}{h} = 100$.

Our results to this problem are given in table 6.11, 6.12.

Mesh Type	$\bar{w}_0$	Π_p
Mesh I	-0.4336	-0.0605
Mesh II	-0.4352	-0.0612
Mesh III	-0.4353	-0.0614
Mesh IV	-0.4353	-0.0614
Kant et al [16]	-0.4344	-

Table 6.11: Validation study for thin plate with mesh refinement for $p = 3$

p	$\bar{w}_0$	Π_p
1	-0.0388	-0.0530
2	-0.4255	-0.0600
3	-0.4353	-0.0614
4	-0.4353	-0.0614
Kant et al [16]	-0.4344	-

Table 6.12: Validation study for thin plate with p refinement for Mesh III

From above tables we can see that:

- The non-dimensionalised displacement converges to -0.4353 and total potential to -0.0614 for mesh refinement level $\geq$ III.
- For fixed mesh refinement level III, and p refinement the results converge with $p \geq 3$.

- The non-dimensional displacement from our study is different from the reference values. This is because, the reference study was done with a fixed refined mesh and convergence study was not done.

PROBLEM 6

Simply supported rectangular laminated plate loaded with uniformly distributed transverse load is analysed here. The material properties of *T300/5208 Graphite/Epoxy (pre-preg)* ($v_f = 0.7$) are given below:

$E_1 = 132.5$ GPa; $E_2 = E_3 = 10.8$ GPa;

$G_{12} = G_{13} = 5.7$ GPa; $G_{23} = 3.4$ GPa;

$\nu_{12} = \nu_{13} = 0.24$; $\nu_{23} = 0.49$;

$X = 229$ mm; $Y = 127$ mm;

Thickness of each ply = 0.127 mm; Ply Orientations $[0/90]_s$;

$q_0 = 6.9 \times 10^{-4}$ MPa

Results are tabulated in table 6.13, 6.14.

It can be observed that:

- The displacement converge to value of -11.5004 with mesh refinement for mesh refinement level $\geq$ III.
- The convergence is with $p \geq 3$ for p refinement in the mesh with III levels of refinement.
- The reference results are obtained for constant mesh and with FSDT model. Also no convergence study was done. We have used HSDT model, which assumes flexiblity over FSDT model.

Mesh Type	$w_0{}^*$	Π_p
Mesh I	-11.7421	-23.9584
Mesh II	-11.5132	-24.2721
Mesh III	-11.5004	-24.4141
Mesh IV	-11.5004	-24.4231
Reddy et al [31]	-11.5000	-

Table 6.13: Validation study for thin plate with mesh refinement for $p = 3$

p	$w_0{}^*$	Π_p
1	-0.0340	-0.0712
2	-10.9555	-23.2155
3	-11.5004	-24.4141
4	-11.5004	-24.4250
Reddy et al [31]	-11.5000	-

Table 6.14: Validation study for thin plate with p refinement for Mesh III

6.2 VALIDATION OF FAILURE CRITERION

The Non-dimensionalised centre deflection corresponding to the first-ply failure load is given by:

$$w_0^* = \frac{w_0}{h}$$

and the non-dimensionalised first-ply failure load (FLD) is given by:

$$FLD = (\frac{p_0}{E_2})(\frac{a}{h})^4$$

For this validation study, mesh topology shown in fig. 6.2 is used.

First an antisymmetric angle ply laminated plate is studied for its first-ply failure load. In second problem, we have analysed symmetric cross ply laminate for its first-ply failure load.

PROBLEM 1

An antisymmetric angle ply laminated plate clamped along all edges and loaded with uniformly distributed transverse load is analysed for first-ply failure load.

The properties are same as in problem 6 of previous section with the change in the ply orientations as $[-45/45/-45/45]$. The material strengths are given as follows:

$X_T = 1515$ MPa; $\quad X_C = 1697$ MPa;

$Y_T = Z_T = 43.8$ MPa; $\quad Y_C = Z_C = 43.8$ MPa;

$R = 67.6$ MPa; $\quad S = T = 86.9$ MPa

Results from our analysis are reported in table 6.15 and 6.16.

In table 6.15-6.18, *Rec I* and *Rec II* denotes failure criterion uses the *recovered stresses* along with Eqn. (5.2) and Eqn. (5.3), respectively. *Fem* denotes *finite element stresses* along with Eqn. (5.3)

From the above tables we can see that:

- For fixed value of p with mesh refinement, the failure load for refinement II is

very high. This is due to locking effect exhibited by plate. Since plate is very thin and clamped along all edges, this effect is more seviour.

- Similar observation can be made for p refinement for p=2.
- With higher levels of refinement in mesh (IV) or high p values the failure loads are near to the reference values.
- The failure loads with recovered stresses are lower compared to failure load obtained by using finite element stresses. For the recovered stresses the failure criterion yields the same failure load with and with out transverse shear stresses.
- The failure locations are different for our study. The problem considered is symmetric in all respect. Hence, locations can also be expected to be symmetric. We are getting the locations on the opposite face as that obtained from reference results.
- The reference results are obtained for a fixed mesh with FSDT model using Lagrangian isoparametric rectangular elements and no convergence study was done.

PROBLEM 2

The problem description is same as previous problem except the lamination scheme. The lamination scheme for this problem is $[0/90]_s$.

Results from our analysis are reported in table 6.17 and 6.18.

The comparison of the results with the reference results yield the same conclusions as before.

Mesh Type	Stress Type	FLD	w_0^*	xco	yco	Ply Number	Location
Mesh II	Rec I	1.771×10^6	-35.09	111.93	2.84	1	Top
	Rec II	1.771×10^6	-35.09	111.93	2.84	1	Top
	Fem	1.223×10^6	-24.25	166.62	93.82	4	Bottom
Mesh III	Rec I	46264.58	-25.77	115.78	1.42	1	Top
	Rec II	46264.58	-25.77	115.78	1.42	1	Top
	Fem	55555.74	-30.94	111.93	0.71	1	Top
Mesh IV	Rec I	37661.66	-23.85	115.35	0.95	1	Top
	Rec II	37661.66	-23.85	115.35	0.95	1	Top
	Fem	41294.01	-26.15	112.79	0.47	1	Top
Reddy et al [31]	Fem	39354.80	-26.79	≈ 125	≈ 125	1	Top

Table 6.15: Validation study for first-ply failure load for [-45/45/-45/45] laminate with h refinement for $p = 2$

p	Stress Type	FLD	w_0^*	xco	yco	Ply Number	Location
2	Rec I	1.771×10^6	-35.09	111.93	2.34	1	Top
	Rec II	1.771×10^6	-35.09	111.93	2.34	1	Top
	Fem	1.223×10^6	-24.25	166.62	93.82	4	Bottom
3	Rec I	38044.02	-25.66	129.31	125.83	1	Top
	Rec II	38044.02	-25.66	129.31	125.83	1	Top
	Fem	35558.73	-24.10	119.62	125.57	1	Top
4	Rec I	32385.21	-21.92	99.68	125.83	1	Top
	Rec II	32385.21	-21.92	99.68	125.83	1	Top
	Fem	29058.74	-19.64	176.87	3.32	1	Top
Reddy et al [31]	Fem	39354.80	-23.79	≈ 125	≈ 125	1	Top

Table 6.16: Validation study for first-ply failure load for [-45/45/-45/45] laminate with p refinement for Mesh II

Mesh Type	Stress Type	FLD	w_0^*	xco	yco	Ply Number	Location
Mesh II	Rec I	1.215×10^6	-24.38	117.06	2.84	4	Bottom
	Rec II	1.215×10^6	-24.38	117.06	2.84	4	Bottom
	Fem	1.173×10^6	-23.53	119.62	1.42	1	Top
Mesh III	Rec I	26955.81	-21.92	115.78	1.42	1	Top
	Rec II	26955.81	-21.92	115.78	1.42	1	Top
	Fem	29899.92	-24.32	117.06	0.71	1	Top
Mesh IV	Rec I	19499.95	-18.41	115.35	126.05	1	Top
	Rec II	19499.95	-18.41	115.35	126.05	1	Top
	Fem	21029.35	-19.85	112.79	126.52	1	Top
Reddy et al [31]	Fem	19050.90	-19.34	≈ 2	≈ 75	1	Top

Table 6.17: Validation study for first-ply failure load for $[0/90]_s$ laminate with h refinement for $p = 2$

p	Stress Type	FLD	w_0^*	xco	yco	Ply Number	Location
2	Rec I	1.215×10^6	-24.38	117.06	2.84	4	Bottom
	Rec II	1.215×10^6	-24.38	117.06	2.84	4	Bottom
	Fem	1.738×10^6	-19.58	119.62	1.42	1	Top
3	Rec I	19423.48	-19.58	109.37	1.42	1	Top
	Rec II	19423.48	-19.58	109.37	1.42	1	Top
	Fem	17588.19	-17.80	119.62	125.57	1	Top
4	Rec I	16823.48	-16.97	119.62	1.42	1	Top
	Rec II	16823.48	-16.97	119.62	1.42	1	Top
	Fem	15676.43	-15.82	119.62	125.57	1	Top
Reddy et al [31]	Fem	19050.90	-19.34	≈ 2	≈ 75	1	Top

Table 6.18: Validation study for first-ply failure load for $[0/90]_s$ laminate with p refinement for Mesh II

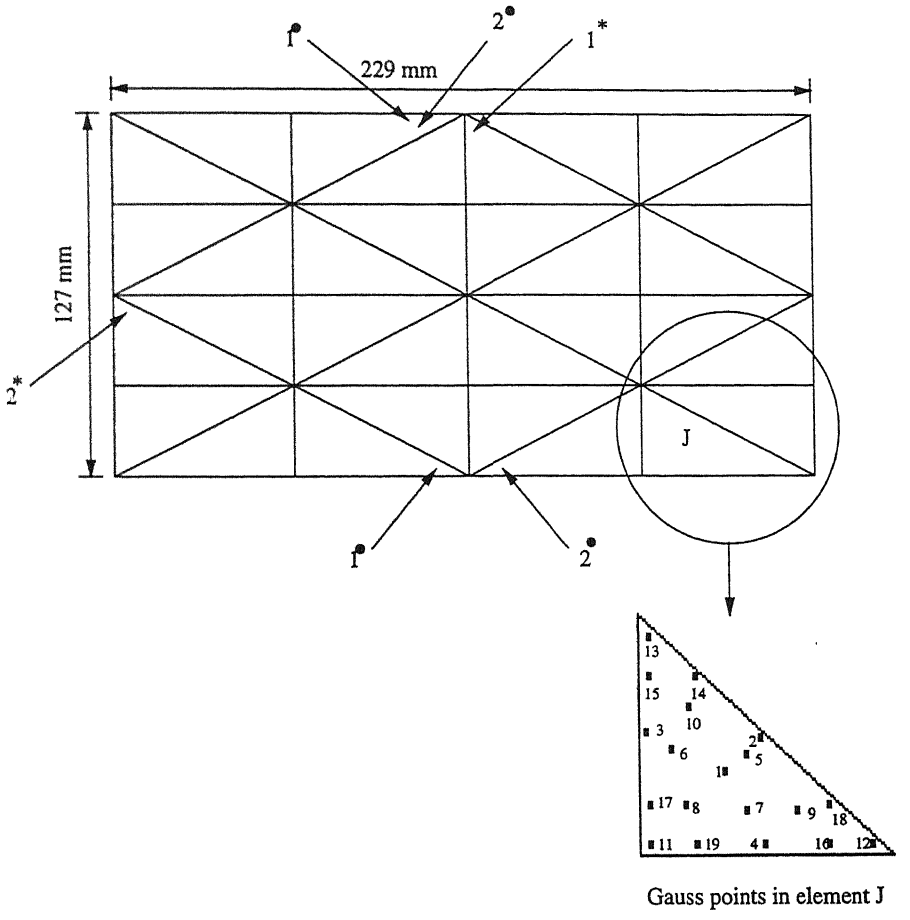

Figure 6.4: Mesh showing the failure points

In fig. 6.4, the gauss points in element J are shown. The failure indices are calculated at these Gauss points, as discussed in the previous chapter. The point 1^* and 2^* denotes the failure locations obtaied by Reddy et al [31] for $[-45/45/-45/45]$ and $[0/90]_s$ laminates, respectively. And $1^\bullet$ and $2^\bullet$ shows the failure locations from our study for $[-45/45/-45/45]$ and $[0/90]_s$ laminates, respectively.

6.3 OPTIMIZATION

Following the validation tests of the previous sections, let us now focus on the problem of shape optimization. Here, through a few typical examples, we will demonstrate the effect of control of discretisation error on the final "optimal" shape of the cut-out.

Note: In each of the problem we start with initial profile with $a = b = Y/8$.

PROBLEM 1:

A rectangular symmetric laminated plate clamped along one of the smaller edge and is loaded transversely with uniformly distributed load with a cut-out is analysed for shape optimization. The lamination scheme is $[0/90]_s$.

Thickness of each layer = 0.127 mm.

$\frac{X}{h} = 10 \quad Y = \frac{X}{2}$

$q_0 = 2.0 N/mm^2$

All laminae are made of *T300/5208 Graphite/Epoxy (pre-preg)* and their properties are given in previous problems.

The optimum cut-out shape results are tabulated in table 6.19.

	a	b	weight	max. index	error (in %)	x coord	y coord
Initial	0.3175	0.3175	12.5865	0.4095	3.6582	2.2109	1.2165
Intermediate	0.5799	0.4109	12.1544	0.7709	4.8672	1.9517	1.3472
Intermediate	0.6015	0.4119	12.1245	0.7899	4.3852	1.9197	1.2083
Optimal	0.6057	0.4100	12.1229	0.7959	4.8293	1.9157	1.2077

Table 6.19: Optimal shape for cut-out in $[0/90]_s$ laminate with out adaptive refinement and p =2

From these results we observe that:

- The errors are below 5% for all the feasible shapes. Hence, adaptive refinement is not needed.

- The failure occurs at the edges of cut-out boundary. The failure is dominated by σ_{yy}. This is in accordance with the the results obtained by Ericson et al [23].

The cut-out shapes during optimization are shown in fig. 6.5

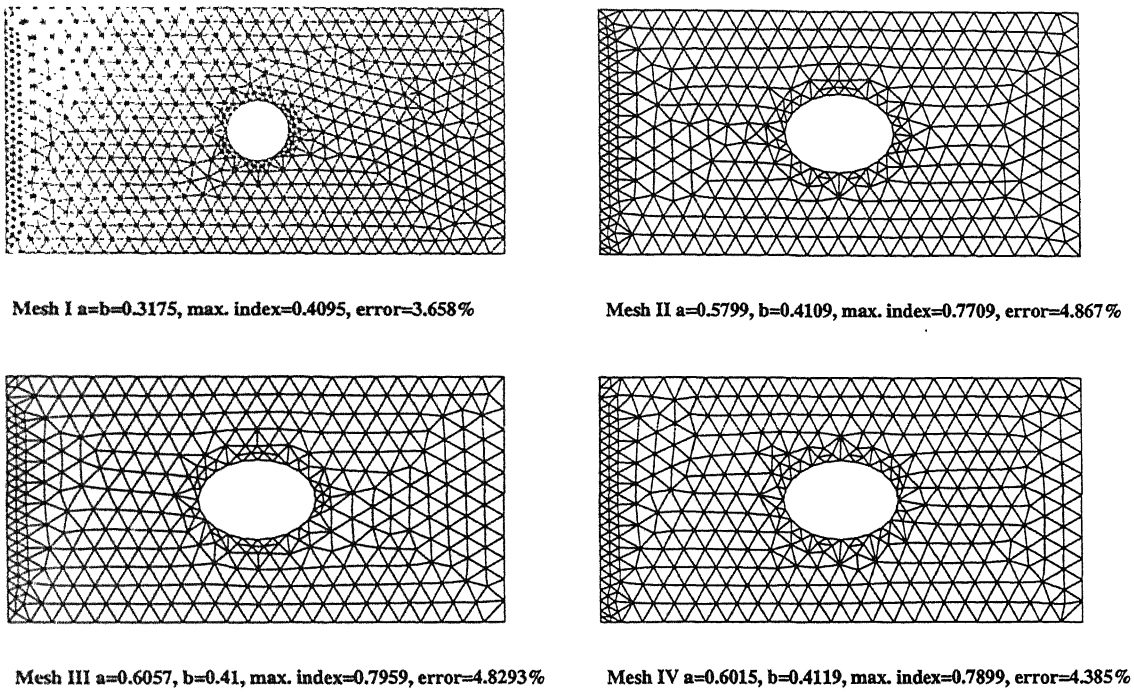

Figure 6.5: Cut-out shapes during optimization

PROBLEM 2:

The problem description is same as above. The lamination scheme is changed to $[45/-45]_s$. $q_0 = 0.22N/mm^2$

The results are tabulated in table 6.20.

From these results we observe that:

- The errors are above 10% in most of the feasible shapes.
- The final optimum shape is the upper bound on the design variables.
- The failure occurs at the edges of cut-out boundary and the location changes.

	a	b	weight	max. index	error (in %)	x coord	y coord
Initial	0.3175	0.3175	12.5865	0.4953	7.1979	0.0740	0.0224
Intermediate	0.8598	0.8808	10.5236	0.3461	11.8820	2.1983	0.4315
Intermediate	1.0122	0.8960	10.0535	0.3939	11.8937	2.1435	0.4188
Optimal	1.0160	1.0160	09.6602	0.7712	15.6503	2.4090	2.3167

Table 6.20: Optimal shape for cut-out in $[45/-45]_s$ laminate with out adaptive refinement and p =2

- The failure is dominated by σ_{yy} and τ_{xy}. This is in accordance with experimental study reported by Herakovich [27].

For optimum shape obtained, now we will see the effect of adaptive refinement on final optimal solution to reduce the error.

The sequence of adaptive mesh refinement is shown in fig 6.6. The errors for these refined meshes are given table 6.21

Refinement level	error (in %)	max. index
First	15.6503	0.7712
Second	15.0825	-
Third	12.4125	-
Fourth	11.0823	-
Fifth	10.4591	1.0089

Table 6.21: Effect of adaptivity on final optimal shape in $[45/-45]_s$ laminate

- Thus, due to adaptive refinement the errors are reduced from 15.6503% to 10.4591% but the failure index is increased from 0.7712 to 1.0089.

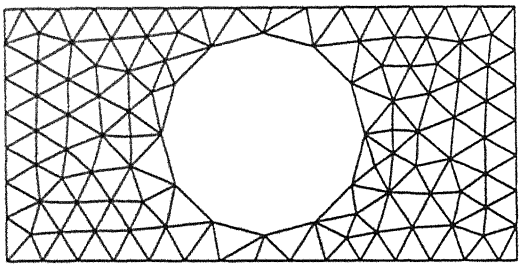

Mesh I

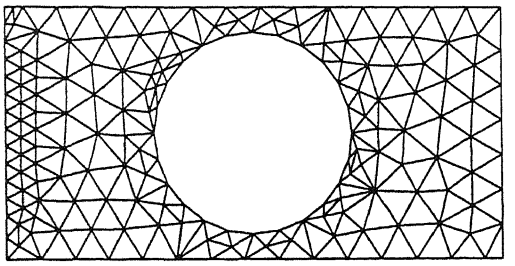

Mesh II

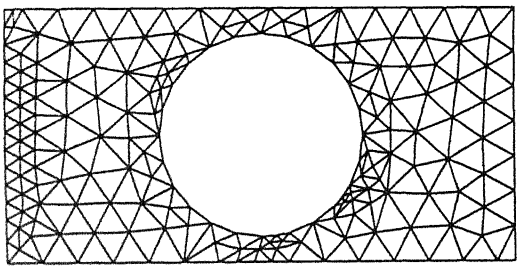

Mesh III

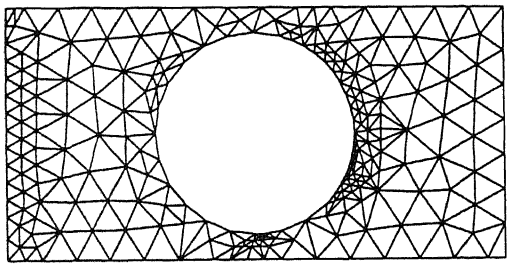

Mesh IV

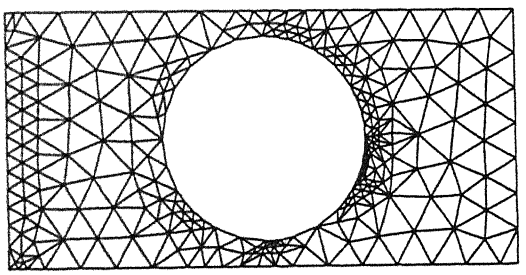

Mesh V

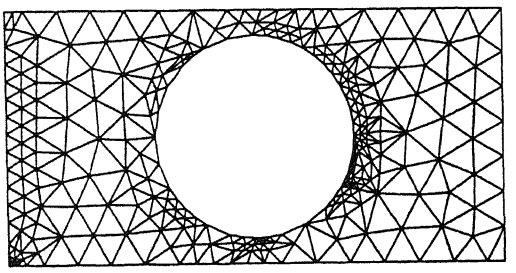

Mesh VI

Figure 6.6: Adaptive refinement in optimum shape

Now we will see the effect of adaptivity when employed through out the optimization process.

The mesh is refined adaptively till either the tolerance in error is reduced below 7% or for five levels of refinement. The comparison of results with and without adaptivity is shown in table 6.22

Adaptivity	a	b	weight	max. index	error (in %)
No	1.0160	1.0160	09.6602	0.7712	15.6503
Yes	0.5248	0.3175	12.3796	0.7978	6.7000

Table 6.22: Effect of adaptivity on optimal shape in $[45/-45]_s$ laminate subjected to transverse loading

Thus, it is seen that:

- The final optimal shape obtained with and without adaptivity are totally different.
- The error for the final optimal shape with adaptive procedure is well below the tolerance mentioned.
- The failure occurs in the cut-out boundary but the location changes.

PROBLEM 3:

A rectangular symmetrically laminated composite plate clamped along a smaller edge and is loaded combinedly with uniformly distributed load, in-plane tensile loading and shear load.

The lamination scheme and laminae properties are as in problem 2.

$$q_0 = 0.15N/mm^2; \quad N_x = 20N/mm; \quad N_{xy} = 0.35N/mm$$

Adaptivity	a	b	weight	max. index	error (in %)
No	1.0155	0.8753	10.1103	0.7997	8.3792
Yes	1.0157	0.8258	10.2681	0.7999	6.4297

Table 6.23: Effect of adaptivity on optimal shape in $[45/-45]_s$ laminate subjected to combined loading

Here, we see that:

- The final optimal shapes obtained with and without adaptivity are near to each other.
- The error in optimum shape obtained with adaptivity is below the specified tolerance.
- The failure occurs in the cut-out boundary but the location changes.

Chapter 7

CONCLUSIONS AND FUTURE SCOPE

7.1 CONCLUSIONS

In this study an attempt has been made to estimate and control the discretisation error, in the analysis of laminated plates with cut-outs. The effect of errors on the evaluated constraint quantities on the final design have also been analysed. From this study, it can be further concluded that:

1. For thick plates, the model used needs moderately refined mesh and approxi mation order is sufficient.

2. For moderately thick plates, proper refinement and approximation orders should be chosen for better convergence.

3. For thin plates, boundary layer effect is severe. Mesh refinements are needed in order to eliminate the effect of locking. Higher apporoximation orders (above three) is also needed in order to reduce the locking effect. Thus, for a thin plate greater care should be taken (with respect to the approximation) in order to ensure reliability of the solution quantities.

4. The recovered stresses seem to be reasonably accurate. A detailed analysis

7.2 FUTURE SCOPE

1. The developed finite element program is modular in nature and can, for a given mesh, element order p, laminate properties, and loadings, give the solution. However, in order to make this code more effective the following modules need to be developed:

   (i) Curved elements are to be mapped with higher order approximation so that it automatically changes the mapping order according to the approximation order used and mapping errors are checked.

   (ii) In the a-posteriori error estimator, recovered stresses are directly used in the further analyses. Instead, a more smoothened stress field can be obtained by averaging the stresses.

   (iii) The optimization technique uses a simple algorithm of complex search method. For sophisticated analysis a suitable Genetic Algorithm can be used.

   (iv) The code is also capable of handling multiple cut-outs. Another module can be developed to observe behaviour of plate with multiple cut-outs.

2. Presently, the code is working well for transverse and in-plane loadings. In future modules for buckling analysis, post-buckling behaviour, eigen value prob lem, free vibration problems, etc can be added.

3. Presently optimization uses 'first-ply failure criterion' as a constraint. Buck ling load can be included as another constraint.

4. The code is capable of handling multiple load cases. It is to be properly activated.

5. The formulation can be generalized to curvilinear coordinates in order to analyze the curved panels and shells also.

6. Code can be extended to include geometric non-linearity to handle large deformat ions.

APPENDIX A

$$\begin{Bmatrix} N_x \\ N_y \\ N_{xy} \\ M_x \\ M_y \\ M_{xy} \\ M_x^* \\ M_y^* \\ M_{xy}^* \\ Q_x \\ Q_y \\ Q_x^* \\ Q_y^* \end{Bmatrix} = \sum_{l=1}^{NL} \begin{bmatrix} [D_m]_{3\times3} & [D_c]_{3\times6} & [0]_{3\times4} \\ [D_c]^T_{6\times3} & [D_b]_{6\times6} & [0]_{6\times4} \\ [0]_{4\times3} & [0]_{4\times6} & [D_s]_{4\times4} \end{bmatrix}_l \begin{Bmatrix} \epsilon_x \\ \epsilon_y \\ \epsilon_{xy} \\ k_x \\ k_y \\ k_{xy} \\ k_x^* \\ k_y^* \\ k_{xy}^* \\ \nu_x \\ \nu_y \\ \nu_x^* \\ \nu_y^* \end{Bmatrix} \tag{1}$$

where,

$$[D_m]_l = \begin{bmatrix} \bar{Q}_{11}H_1 & \bar{Q}_{12}H_1 & \bar{Q}_{16}H_1 \\ \bar{Q}_{21}H_1 & \bar{Q}_{22}H_1 & \bar{Q}_{26}H_1 \\ \bar{Q}_{16}H_1 & \bar{Q}_{26}H_1 & \bar{Q}_{66}H_1 \end{bmatrix}_l$$

$$[D_c]_l = \begin{bmatrix} \bar{Q}_{11}H_2 & \bar{Q}_{12}H_2 & \bar{Q}_{16}H_2 & \bar{Q}_{11}H_4 & \bar{Q}_{12}H_4 & \bar{Q}_{16}H_4 \\ \bar{Q}_{21}H_2 & \bar{Q}_{22}H_2 & \bar{Q}_{26}H_2 & \bar{Q}_{11}H_4 & \bar{Q}_{12}H_4 & \bar{Q}_{16}H_4 \\ \bar{Q}_{16}H_2 & \bar{Q}_{26}H_2 & \bar{Q}_{66}H_2 & \bar{Q}_{11}H_4 & \bar{Q}_{12}H_4 & \bar{Q}_{16}H_4 \end{bmatrix}_l$$

$$[D_b]_l = \begin{bmatrix} \bar{Q}_{11}H_3 & \bar{Q}_{12}H_3 & \bar{Q}_{16}H_3 & \bar{Q}_{11}H_5 & \bar{Q}_{12}H_5 & \bar{Q}_{16}H_5 \\ \bar{Q}_{21}H_3 & \bar{Q}_{22}H_3 & \bar{Q}_{26}H_3 & \bar{Q}_{11}H_5 & \bar{Q}_{12}H_5 & \bar{Q}_{16}H_5 \\ \bar{Q}_{16}H_3 & \bar{Q}_{26}H_3 & \bar{Q}_{66}H_3 & \bar{Q}_{11}H_5 & \bar{Q}_{12}H_5 & \bar{Q}_{16}H_5 \\ \bar{Q}_{11}H_5 & \bar{Q}_{12}H_5 & \bar{Q}_{16}H_5 & \bar{Q}_{11}H_7 & \bar{Q}_{12}H_7 & \bar{Q}_{16}H_7 \\ \bar{Q}_{21}H_5 & \bar{Q}_{22}H_5 & \bar{Q}_{26}H_5 & \bar{Q}_{11}H_7 & \bar{Q}_{12}H_7 & \bar{Q}_{16}H_7 \\ \bar{Q}_{16}H_5 & \bar{Q}_{26}H_5 & \bar{Q}_{66}H_5 & \bar{Q}_{11}H_7 & \bar{Q}_{12}H_7 & \bar{Q}_{16}H_7 \end{bmatrix}_l$$

$$[D_s]_l = \begin{bmatrix} \bar{Q}_{55}H_1 & \bar{Q}_{45}H_1 & \bar{Q}_{55}H_3 & \bar{Q}_{45}H_3 \\ \bar{Q}_{45}H_1 & \bar{Q}_{44}H_1 & \bar{Q}_{45}H_3 & \bar{Q}_{44}H_3 \\ \bar{Q}_{55}H_3 & \bar{Q}_{45}H_3 & \bar{Q}_{55}H_5 & \bar{Q}_{45}H_5 \\ \bar{Q}_{45}H_3 & \bar{Q}_{44}H_3 & \bar{Q}_{45}H_5 & \bar{Q}_{44}H_5 \end{bmatrix}_l$$

in which,

$H_i = \frac{1}{i}\left({t^i}_l - {t^i}_{l-1} \right)$, i = 1,2,3,4,5,7

And

$$[D_r] = \begin{bmatrix} [D_m] & [D_c] & 0 \\ [D_c]^T & [D_b] & 0 \\ 0 & 0 & [D_s] \end{bmatrix} \tag{2}$$

APPENDIX B

$$[N] = \begin{bmatrix} N_1 & 0 & 0 & ... & N_2 & 0 & 0 & ... \\ 0 & N_1 & 0 & ... & 0 & N_2 & 0 & ... \\ 0 & 0 & N_1 & ... & 0 & 0 & N_2 & ... \\ \vdots & & & & \vdots & & \vdots & \end{bmatrix} \tag{1}$$

$$[B_m] = \begin{bmatrix} N_{i,x} & 0 & 0 & 0 & 0 & 0 & 0 \\ 0 & N_{i,y} & 0 & 0 & 0 & 0 & 0 \\ N_{i,y} & N_{i,x} & 0 & 0 & 0 & 0 & 0 \end{bmatrix} \tag{2}$$

$$[B_b] = \begin{bmatrix} 0 & 0 & 0 & N_{i,x} & 0 & 0 & 0 \\ 0 & 0 & 0 & 0 & N_{i,y} & 0 & 0 \\ 0 & 0 & 0 & N_{i,y} & N_{i,x} & 0 & 0 \\ 0 & 0 & 0 & 0 & 0 & N_{i,x} & 0 \\ 0 & 0 & 0 & 0 & 0 & 0 & N_{i,y} \\ 0 & 0 & 0 & 0 & 0 & N_{i,y} & N_{i,x} \end{bmatrix} \tag{3}$$

$$[B_s] = \begin{bmatrix} 0 & 0 & N_{i,x} & 1 & 0 & 0 & 0 \\ 0 & 0 & N_{i,y} & 0 & 1 & 0 & 0 \\ 0 & 0 & 0 & 0 & 0 & 3 & 0 \\ 0 & 0 & 0 & 0 & 0 & 0 & 3 \end{bmatrix} \tag{4}$$

$$\{d^T\} = \{\delta_1^T, \delta_2^T, ...\delta_{NN}^T\} \tag{5}$$

Bibliography

[1] Won J. Park. "An Optimal Design of Simple Symmetric Laminates Under the First Ply Failure Criterion." *Journal of Composite Materials, Vol. 16, July 1982 pp. 341-355.*

[2] Hisao Fukunaga and Hideki Sekine. "Optimum Design of Composite Structures for Shape, Layer Angle and Layer Thickness Distributions." *Journal of Composite Materials, Vol. 27, No. 15/ 1993 pp. 1479-1492.*

[3] Chin Fang and George S. Springer. "Design of Composite Laminates by a Monte Carlo Method." *Journal of Composite Materials, Vol. 27, No. 7/ 1993 pp. 721-753.*

[4] Stevan Maksimovic. "Some Computational and Experimental Aspects of Optimal Process of Composite Structures." *Composite Structures 17 (1990) pp. 237-258.*

[5] S. Mahadevan and X. Liu. "Probabilistic Optimum Design of Composite Laminates." *Journal of Composite Materials, Vol. 32, No. 1/1998 pp. 68-82.*

[6] C. A. Conceicao Antonio, A. Torres Marques and Alfredo V. Soeiro. "Optimization of Laminated Composite Structures Using a Bilevel Strategy." *Composite Structures 33 (1995) pp. 193-200.*

[7] Serge Abrate. "Optimal Design of Laminated Plates and Shells." *Composite Structures 29 (1994) pp. 269-286.*

[8] T. Y. Kam, F. M. Lai and S. C. Liao. "Minimum Weight Design of Laminated Composite Plates Subject to Strength Constraint." *AIAA Journal, Vol. 34, No. 8, August 1996 pp. 1699-1708.*

[9] Yung S. Shin, Raphael T. Haftka, Layne T. Watson and Raymond H. Plaut. "Design of Laminated Plates for Maximum Buckling Load," *Journal of Composite Materials, Vol. 23-April 1989 pp. 348-369.*

[10] S. Adali, A. Richter, V. E. Verijenko and E. B. Summers. "Optimal Design of Hybrid Laminates with Discrete Ply Angles for Maximum Buckling Load and Minimum Cost." *Composite Structures 32 (1995) pp. 409-415.*

[11] S. Adali, M. Walker and V. E. Verijenko. "Multiobjective Optimization of Laminated Plates for Maximum Prebuckling, Buckling and Postbuckling Strength using Continuous and Discrete Ply Angles." *Composite Structures 35 (1996) pp. 117-130.*

[12] S. Nagendra, R. T. Haftka and Z. Gurdal. "Design of a Blade-Stiffened Composite Panel with a Hole." *Composite Structures 18 (1991) pp. 195-219.*

[13] N. K. Naik and V. K. Ganesh. "Optimum Design Studies on FRP Beams with Holes." *Composite Structures 24 (1993) 59-66.*

[14] M. E. Botkin. "Shape Optimization with Buckling and Stress Constraints." *AIAA Journal, Vol. 34, No. 2 Technical Notes 1996 pp. 423-425.*

[15] K. Sivakumar, K. Deb and N. G. R. Iyengar. "Optimum Design of Laminated Composite Plates with Dynamic Constraints." *Ph. D. dissertation at Indian Institute of Technology, Kanpur, India. 1998.*

[16] B. N. Pandya, Mallikarjuna and T. Kant. *Ph. D. dissertation at Indian Institute of Technology, Bombay, India. Private Publication.*

[17] B. D. Agarwal and L. J. Broutman. Analysis and Performance of Fiber Composites. John Willy and Sons, New Delhi.

[18] Robert M. Jones. Mechanics of Composite Materials. Scripta Book Company, McGraw-Hill Kogakusha, Ltd. New Delhi.

[19] Ricardo L. Actis, Barna A. Szabo and Christoph Schwab. "Hierarchic Models for Laminated Plates and Shells." *Review print, Private publication, Nov. 30 (1997).*

[20] Chandra Shekhar Upadhyay. "Computer-Based Analysis of Error Estimation and Superconvergence in Finite Element Computations." *Ph. D. dissertation at Texas A&M University, Texas. May 1997.*

[21] Kalyanmoy Deb. Optimization for Engineering Design, Algorithms and Examples. Prentice Hall of India Private Limited, New Delhi, 1998.

[22] Stephen W. Tsai, Edward M. Wu. "A General Theory of Strength for Anisotropic Materials." *Journal of Composite Materials, Vol. 5 - January 1971 pp. 58-80.*

[23] K. Ericson, M. Persson, L. Carlsson and A. Gustavsson. "On the Prediction of the Initiation of Delamination in a $[0/90]_s$ Laminate with a Circular Hole." *Journal of Composite Materials, Vol. 18 - September 1984 pp. 495-506.*

[24] P.W.M. Peters. "The Strength Distribution of 90° Plies in 0/90/0 Graphite-Epoxy Laminates." *Journal of Composite Materials, Vol. 18 - November 1984 pp. 545-556.*

[25] Peter W. Manders, Tsu-Wei Chou, Frank R. Jones and John W. Rock. "Statistical Analysis of Multiple Fracture in 0°/90°/0° Glass Fibre/Epoxy Resin Laminates." *Journal of Materials Science 18 (1983) pp. 2876-2889.*

[26] C. Soutis, N.A. Fleck and P.A. Smith. "Failure Prediction Technique for Compression Loaded Carbon Fibre-Epoxy Laminate with Open Holes." *Journal of Composite Materials, Vol. 25 - November 1991 pp. 1476-1498.*

[27] Carl T. Herakovich. "Mechanics of Fibrous Composites." John Wiley and Sons, Inc. Delhi 1998.

[28] George H. Staab. Laminar Composites. Butterworth Heinemann, New Delhi.

[29] J. N. Reddy and A. Miravete. " Practical Analysis of Composite Laminates." CRC Press, New York, 1995.

[30] J. N. Reddy. " Mechanics of Composite Materials. Selected Works of Nicholas J. Pagano. " Kluwer Academic Publishers, 1994.

[31] Y. S. N. Reddy and J. N. Reddy. "Linear and Non-Linear Failure Analysis of Composite Lamintaes with Transverse Shear." *Composite Science and Technology 44 (1992) pp. 227-255.*

[32] S. B. Singh, Ashwini Kumar and N. G. R. Iyengar. "Progressive Failure of Symmetrically Laminated Plates under Uni-axial Compression." *Structural Engg. and Mech. 5 (1997) pp. 433-450.*

133651

Date Slip

The book is to be returned on the date last stamped.

.....	.....
.....	.....
.....	.....
.....	.....
.....	.....
.....	.....
.....	.....
.....	.....
.....	.....
.....	.....
.....	.....